

# Bayesian inference for spline-based hidden Markov models

Sida Chen

Department of Statistics, University of Warwick  
and

Bärbel Finkenstädt Rand

Department of Statistics, University of Warwick

November 4, 2020

## Abstract

B-spline-based hidden Markov models (HMMs), where the emission densities are specified as mixtures of normalized B-spline basis functions, offer a more flexible modelling approach to data than conventional parametric HMMs. We introduce a fully Bayesian framework for inference in these nonparametric models where the number of states may be unknown along with other model parameters. We propose the use of a trans-dimensional Markov chain inference algorithm to identify a parsimonious knot configuration of the B-splines while model selection regarding the number of states can be performed within a parallel sampling framework. The feasibility and efficiency of our proposed methodology is shown in a simulation study. Its explorative use for real data is demonstrated for activity acceleration data in animals, i.e. whitetip-sharks. The flexibility of a Bayesian approach allows us to extend the modelling framework in a straightforward way and we demonstrate this by developing a hierarchical conditional HMM to analyse human accelerator activity data to focus on studying small movements and/or inactivity during sleep.

*Keywords:* Bayesian hidden Markov models; Free-knot splines; Reversible-jump MCMC; Model selection; Animal movement data; Accelerometer data

# 1 Introduction

The class of hidden Markov models (HMMs) offers an important modelling approach for extracting information from sequential data; illustrations of applications and an extended bibliography can be found, for example, in Cappé et al. (2005) and Zucchini et al. (2016). A basic  $N$ -state HMM consists of a discrete-time stochastic process  $(x_t, y_t)$  with  $x_t \in \{1, \dots, N\}$  and  $y_t | x_t \sim f_{x_t}(y_t)$ , where  $\{x_t\}$  is unobserved and assumed to be distributed as an  $N$ -state time-homogeneous Markov chain, and, conditionally on  $\{x_t\}$ , the  $y_t$ 's are independent with state-dependent *emission* densities  $f_i$ . They are usually assumed to belong to a parametric family of distributions, such as the normal or gamma family. It is however recognized that such parametric choices are not always well justified where misspecification can lead to seriously erroneous inference on the number of hidden states and on the classification of the observations to the states (Yau et al., 2011; Gassiat et al., 2016a; Pohle et al., 2017). Nonparametric approaches may serve as exploratory tools to investigate the suitability of a parametric family of emission distributions (Langrock et al., 2015). Considerable effort has been invested in the use of semi- and nonparametric emission distributions such as proposed in Piccardi and Pérez (2007) for activity recognition in videos, Yau et al. (2011) for the analysis of genomic copy number variation, Langrock et al. (2015, 2018) for modelling animal movement and Kang et al. (2019) for delineating the pathology of Alzheimer's disease, to mention some examples. Theoretical properties for inference in such models have been studied by Alexandrovich et al. (2016) who proved that model parameters as well as the order of the Markov chain are identifiable (up to permutations of the hidden states labels) if the transition probability matrix has full rank and is ergodic, and if the emission distributions are distinct. These conditions are fairly generic and in practice will usually be satisfied. We also refer to Gassiat et al. (2016a,b) for further useful identifiability results and to Vernet et al. (2015), Lehéricy (2018), De Castro et al. (2017) and references therein for further theoretical results for inference in this nonparametric setting.

The increased flexibility and modelling accuracy of a nonparametric approach comes at the cost of a higher computational complexity needed for inference. For instance, the computational cost of the forward algorithm of Rabiner (1989) for kernel-based HMMs

(Piccardi and Pérez, 2007) is subject to quadratic growth with sample size  $n$  and thus can be prohibitive for long time series data. Also for mixtures of Dirichlet process (MDPs) HMMs (Yau et al., 2011) the increased complexity of the model space poses severe computational challenges on the sampling methods (Hastie et al., 2015). We focus on spline-based HMMs which are attractive for real applications as they exploit the strengths of two powerful tools, namely the forward algorithm for efficient and exact likelihood evaluation, and the flexibility of B-splines for estimating the emission densities, while retaining a simple model formulation. A frequentist approach for inference based on penalized B-splines was introduced by Langrock et al. (2015, 2018). Their methods require a full specification of the number and positions of knots which may influence the computational cost and the estimation results as, in practice, a large number of equidistant knots need to be fixed to ensure some flexibility. Considering the computational challenges their approach is only feasible for models with a small number of states which may severely limit its applicability.

The selection of the state-specific smoothing parameters and the quantification of uncertainty of parameter estimates to date remain open and challenging inferential tasks. Current methods rely on cross-validation and parametric bootstrap techniques, which are extremely computationally intensive and can be numerically unstable especially for increasing  $N$ . Other nonparametric approaches (see Piccardi and Pérez (2007); Yau et al. (2011), Lehéricy (2018)) also require the number of states to be known or fixed in advance. This will not be realistic in scenarios where estimating  $N$  is in itself of scientific interest. While the problem of order estimation has been extensively studied for parametric HMMs (see, e.g., Celeux and Durand (2008); Robert et al. (2000) and Pohle et al. (2017)), few theoretical or practical results have been obtained for the nonparametric case. We note that Lehéricy et al. (2019) recently proposed two different estimators for  $N$  which are consistent in a fairly general setup. Although theoretically attractive, both estimators are difficult to implement. An alternative strategy is to use Bayesian nonparametric techniques to allow for a potentially infinitely large state space, see Fox et al. (2011) for an illustration. In this paper, however, we will consider HMMs with a finite and fixed state space whose cardinality  $N$  may be unknown.

To the best of our knowledge, spline-based methods have not previously been used in a Bayesian HMM. We therefore propose and develop a fully Bayesian methodology that jointly estimates the spline functions for the emission densities and other HMM parameters, and provides a consistent and principled framework for quantifying uncertainties associated with model parameters. We develop a trans-dimensional or reversible jump Markov chain Monte Carlo (RJMCMC) algorithm (Green, 1995) incorporating additional techniques, such as a reparametrization scheme to enhance the sampling efficiency, and an adaptive knot selection scheme which modifies and extends ideas considered in a different modelling context, see for instance Biller (2000), DiMatteo et al. (2001) for Bayesian adaptive smoothing and more recently Sharef et al. (2010) for baseline hazard modelling. We address model selection of  $N$  through a parallel sampling scheme which is straightforward to implement and computationally efficient as it only involves simultaneous and independent runs of the proposed algorithm for candidate values of  $N$ , from which quantities such as posterior model probabilities or the deviance information criterion (DIC) (Spiegelhalter et al., 2002) for each model can be estimated. A further advantage of a Bayesian inference framework is that the modularity of its components can be used to perform inference rigorously in a more complex hierarchical model. We will demonstrate this by developing a conditional HMM for human activity data to focus on the state of smallest movements which includes periods of sleep.

The paper is structured as follows: Section 2 provides the details of a Bayesian formulation of the spline-based HMM, Section 3 details the structure of the RJ MCMC algorithm, Section 4 outlines the parallel sampling method for model selection and Section 5 examines the performance of the proposed methods in various simulation settings. Section 6 illustrates our methods on both animal and human activity data. The final section provides a discussion and directions for further work.

## 2 A Bayesian HMM with spline-based emissions

Assume that the emission densities  $f_1, \dots, f_N$  can be approximated by mixtures of standardized cubic B-spline basis functions with knots located between boundary knots  $a$  and

$b$  (assumed fixed) (De Boor, 2001; Langrock et al., 2015). Let  $(K, R_K)$  denote the knot configuration where  $K$  equals the number of interior knots with location given by the  $K$ -dimensional vector  $R_K = (r_1, \dots, r_K)$ , with  $a = r_0 < r_1 < \dots < r_K < r_{K+1} = b$ . For computational reasons (Friedman et al. (2001)) we augment the knot sequence such that  $\bar{R}_K = (r_{-3}, r_{-2}, r_{-1}, a, R_K, b, r_{K+2}, r_{K+3}, r_{K+4})$ , where  $r_{-3} = r_{-2} = r_{-1} = a$  and  $b = r_{K+2} = r_{K+3} = r_{K+4}$ . Thus  $K = k$  corresponds to the case of  $k + 4$  B-spline basis functions, and we assume  $K \geq 2$  for identifiability. Under these settings  $f_i$  is formulated as

$$f_i(y) = \sum_{k=1}^{K+4} a_{i,k} B_k(y), \quad i = 1, \dots, N, \quad (1)$$

where  $B_k(y)$ ,  $k = 1, \dots, K+4$ , denotes the  $k$ -th normalized (such that it integrates to one) B-spline basis function of degree 3 for the knot sequence  $\bar{R}_K$  and the  $a_{i,k}$  are the corresponding coefficients such that  $\sum_{k=1}^{K+4} a_{i,k} = 1$  and  $a_{i,k} \geq 0$ , for all  $k = 1, \dots, K + 4$ . In the time-homogeneous case the class of HMMs is fully specified by the initial state distribution,  $\delta = (\delta_1, \dots, \delta_N)$ , with  $\delta_i = P(x_1 = i)$ , the transition probability matrix,  $\Gamma = (\gamma_{i,j})_{i,j=1,\dots,N}$ , with  $\gamma_{i,j} = P(x_t = j | x_{t-1} = i)$ , and the emission densities defined in (1). The likelihood given observations  $y^{(n)} = (y_1, \dots, y_n)$  can be evaluated in  $O(N^2 n)$  steps using the forward algorithm (see Zucchini et al. (2016))

$$L(K, R_K, \delta, A_K, \Gamma | y^{(n)}) = \delta P(y_1) \Gamma P(y_2) \cdots \Gamma P(y_n) \mathbf{1}, \quad (2)$$

where  $P(y_t)$  is a diagonal matrix with  $i$ -th diagonal entry given by  $f_i(y_t)$ ,  $\mathbf{1}$  is an  $N$  column vector of ones, and  $A_K$  denotes the set of spline coefficients  $a_{i,k}$  ( $i = 1, \dots, N, k = 1, \dots, K + 4$ ). We assume the following factorization of the joint density of model parameters and observations

$$f(K, R_K, \delta, A_K, \Gamma, y^{(n)}) = f(K) f(\delta) f(\Gamma) f(R_K | K) f(A_K | K) f(y^{(n)} | K, R_K, \delta, A_K, \Gamma), \quad (3)$$

where here, and throughout this paper, we shall use  $f(\cdot | \cdot)$  as a generic notation to represent conditional densities as specified by their arguments. We assume a uniform prior on  $\{2, \dots, K_{max}\}$  for  $K$ , with  $K_{max}$  fixed to 50 in our examples where a preliminary study suggests that this is usually large enough to cover the support of  $K$ . Clearly other default

values such as  $n$  may be used instead. As there is no a-priori reason to favour knots at any particular positions, we propose that the  $r_k$  are taken to be the  $k$ -th order statistics of  $K$  independent uniform random variables on  $[a, b]$ , i.e.  $f(R_K|K) = \frac{K!}{(b-a)^K}$ . The state-specific spline coefficients  $(a_{i,1}, \dots, a_{i,K+4})$ ,  $i = 1, \dots, N$ , are reparametrized as

$$a_{i,j} = \frac{\exp(\tilde{a}_{i,j})}{\sum_{l=1}^{K+4} \exp(\tilde{a}_{i,l})}, \quad \tilde{a}_{i,j} \in \mathbb{R},$$

so that the positivity and sum-to-one constraints will not hinder the design of our RJ moves. The fact that the  $\tilde{a}_{i,j}$  are not identifiable is not of concern as we are only interested in the  $a_{i,j}$ , which remain identifiable, and in this way the mixing of the MCMC may be improved (Cappé et al., 2003). We choose to use a log-gamma prior with shape parameter  $\zeta$  and rate parameter 1 on the  $\tilde{a}_{i,j}$ , i.e.  $\exp(\tilde{a}_{i,j}) \sim \text{gamma}(\zeta, 1)$ , giving a symmetric Dirichlet, i.e.  $\text{Dir}(\zeta, \dots, \zeta)$  distribution on the corresponding  $(a_{i,1}, \dots, a_{i,K+4})$ . We choose a vague Gamma(1,1) hyper-prior on  $\zeta$  to reflect our uncertainty on its value. Similarly we reparametrize each row of the transition probability matrix as  $\gamma_{i,j} = \frac{\tilde{\gamma}_{i,j}}{\sum_{l=1}^N \tilde{\gamma}_{i,l}}$ ,  $\tilde{\gamma}_{i,j} > 0$ , and place a vague gamma prior on the  $\tilde{\gamma}_{i,j}$ , i.e.  $f(\tilde{\gamma}_{i,j}) = \text{gamma}(\epsilon_1, 1)$ , which gives a  $\text{Dir}(\epsilon_1, \dots, \epsilon_1)$  distribution on  $(\gamma_{i,1}, \dots, \gamma_{i,N})$ . Also the initial distribution  $\delta$  is reparametrized as  $\delta_i = \frac{\tilde{\delta}_i}{\sum_{l=1}^N \tilde{\delta}_l}$ ,  $\tilde{\delta}_i > 0$ , and the prior distribution on  $\tilde{\delta}_i$  is chosen to be  $\text{gamma}(\epsilon_2, 1)$ . The  $\tilde{a}_{i,j}$ ,  $\tilde{\gamma}_{i,j}$  and  $\tilde{\delta}_i$  are assumed to be a-priori independent. The joint density with all the reparametrizations becomes

$$f(\zeta, K, R_K, \tilde{\delta}, \tilde{A}_K, \tilde{\Gamma}, y^{(n)}) = f(\zeta)f(K)f(\tilde{\delta})f(\tilde{\Gamma})f(R_K|K)f(\tilde{A}_K|K, \zeta)f(y^{(n)}|K, R_K, \tilde{\delta}, \tilde{A}_K, \tilde{\Gamma}), \quad (4)$$

where  $\tilde{\delta} = (\tilde{\delta}_1, \dots, \tilde{\delta}_N)$ ,  $\tilde{\Gamma} = (\tilde{\gamma}_{i,j})_{i,j=1,\dots,N}$  and  $\tilde{A}_K$  represents the set of  $\tilde{a}_{i,k}$  ( $i = 1, \dots, N, k = 1, \dots, K + 4$ ). Note that our HMM likelihood and parameter priors are invariant to relabelling the hidden states, and thus the target posterior density is defined on  $N!$  subspaces, one for each permutation of the labels of the hidden states.

### 3 The RJMCMC algorithm

Our aim is to obtain realisations from the posterior distribution of  $(K, R_K, \delta, A_K, \Gamma)$ , which can be achieved by simulating from the joint posterior density (4). To allow for model

searches between parameter subspaces of different dimensionality, we develop a RJMCMC algorithm which combines Metropolis-Hastings (MH) steps with birth and death moves of the spline knot points. The structure of our algorithm is listed in Algorithm 1, where  $b_K = \mathbf{I}(K = 2) + 0.5 \times \mathbf{I}(3 \leq K < K_{max})$  and  $\mathbf{I}(\cdot)$  is the indicator function. Steps (a)-(e) propose moves within a dimension while the last step proposes a birth or death step which changes the model dimension. Here we give the rules for each of the updating steps while further details regarding the validity and implementation of the algorithm are provided in the appendix. Throughout this section we assume that  $N$  is fixed noting that model selection will be considered in section 4.

---

**Algorithm 1:** Reversible jump MCMC algorithm for spline-based HMMs

---

```

Initialize  $K, R_K, \zeta, \tilde{\delta}, \tilde{A}_K, \tilde{\Gamma}$  ;
for  $i=1, \dots, T$  do
    (a) update the knot location vector  $R_K$ ;
    (b) update the set of B-spline coefficients  $A_K$  (via  $\tilde{A}_K$ );
    (c) update the hyperparameter  $\zeta$ ;
    (d) update the initial distribution  $\delta$  (via  $\tilde{\delta}$ );
    (e) update the transition probability matrix  $\Gamma$  (via  $\tilde{\Gamma}$ );
    draw  $U \sim U(0, 1)$ ;
    if  $U < b_K$  then
        | consider the birth of a knot point in the B-spline representation in (1);
    else
        | consider the death of a knot point in the B-spline representation in (1);
    end
end

```

---

### 3.1 Metropolis-Hastings moves

The moves in steps (a)-(e) are of MH type and are conditioned on the current number of knot points  $K$ . In step (a) a knot  $r_{k^*}$  is chosen uniformly from a set of existing knots

$\{r_1, \dots, r_K\}$  and proposed to be moved to a candidate point,  $r_c$ , which is generated from a normal distribution with mean  $r_{k^*}$  and standard deviation  $\tau_1$ , truncated to  $[a, b]$  (DiMatteo et al., 2001). The proposal in step (b) is generated by a random walk on the  $\tilde{a}_{i,j}$  ( $i = 1, \dots, N; j = 1, \dots, K + 4$ ), i.e.  $\tilde{a}'_{i,j} = \tilde{a}_{i,j} + \rho_{i,j}$ , where  $\rho_{i,j} \sim \mathcal{N}(0, \tau_2^2)$ . In step (c) we update  $\zeta$  via a log-normal random walk  $\log(\zeta') = \log(\zeta) + \nu$ , where  $\nu \sim \mathcal{N}(0, \tau_3^2)$ . Similarly, in steps (d) and (e), the proposed moves on the  $\tilde{\delta}_i$  and  $\tilde{\gamma}_{i,j}$  are  $\log(\tilde{\delta}'_i) = \log(\tilde{\delta}_i) + \beta_i$  and  $\log(\tilde{\gamma}'_{i,j}) = \log(\tilde{\gamma}_{i,j}) + \eta_{i,j}$ , where  $\beta_i \sim \mathcal{N}(0, \tau_4^2)$ ,  $\eta_{i,j} \sim \mathcal{N}(0, \tau_5^2)$ ,  $i = 1, \dots, N$  and  $j = 1, \dots, N$ . The variance parameters  $\tau_1, \dots, \tau_5$  may be regarded as tuning parameters that need to be adjusted (e.g. in pilot runs or during the burn-in period) to achieve a satisfactory mixing of the chain.

## 3.2 Birth and death moves

The birth, or death, moves increase, or decrease, the number of knots, or equivalently, the number of B-spline basis elements. Our design extends the ideas in DiMatteo et al. (2001) and Sharef et al. (2010) to the framework of HMMs. We make a random choice between birth and death with probabilities  $b_K$  and  $d_K = 1 - b_K$ , respectively. In the birth move, we select a knot,  $r_{b^*}$ , at random from the existing knots and create a candidate new knot,  $r_c$ , by drawing from a normal distribution (truncated to  $[a, b]$ ) with mean  $r_{b^*}$  and standard deviation  $\tau(R_K, b^*)$ , where  $\tau$  is chosen as a function having the form  $(r_{b^*+1} - r_{b^*-1})^\alpha$  and  $\alpha$  is a positive real constant. The intuition here is that a new knot is more likely to be needed in locations where existing knots are relatively 'dense'. To complete the birth step we update the corresponding spline coefficients, which now has dimension  $K + 5$  for each state. Here, our design is guided by the deterministic *knot insertion rule* De Boor (2001) which allows for a new knot to be inserted without changing the shape of the overall B-spline curve, noting that in our context this exact relationship become approximate as we are working with normalized basis functions. We extend the scheme by adding more degrees of freedom such that the dimension matching condition required for the RJ MCMC algorithm is fulfilled. More specifically, for the birth of a candidate knot point  $r_c \in (r_{n^*}, r_{n^*+1})$ , the associated



spline parameters  $\tilde{a}'_{i,j}$ , for  $i = 1, \dots, N$ , are created as

$$\tilde{a}'_{i,j} = \begin{cases} \tilde{a}_{i,j} & 1 \leq j \leq n^* + 1 \\ c_j \tilde{a}_{i,j} + (1 - c_j) \tilde{a}_{i,j-1} & n^* + 1 < j < n^* + 4 \\ u_i \tilde{a}_{i,j} + (1 - u_i) \tilde{a}_{i,j-1} & j = n^* + 4 \\ \tilde{a}_{i,j-1} & n^* + 4 < j \leq K + 5 \end{cases} \quad (5)$$

where  $c_j = \frac{r_c - r_{j-4}}{r_{j-1} - r_{j-4}}$  and  $u_i \stackrel{iid}{\sim} U(0, 1)$ . Here the  $\tilde{a}'_{i,j}$  are generated from the deterministic rule in De Boor (2001), except for  $\tilde{a}'_{i,n^*+4}$  where one degree of freedom is introduced through  $u_i$ . This way of updating allows us to effectively use knowledge from current spline parameters, while also allowing for a possible improvement on the fit resulting from the introduction of a new knot point. The parameters in  $\tilde{\delta}$  and  $\tilde{\Gamma}$  are unchanged for this move. Next, consider the death of a knot point and suppose that the current model has knot configuration  $(K, R_K)$ . A knot,  $r_{d^*}$ , is chosen at random from the set of existing knots  $\{r_1, \dots, r_K\}$  and then deleted. The spline parameters associated with this move are updated according to the inverse transformation of (5):

$$\tilde{a}'_{i,j} = \begin{cases} \tilde{a}_{i,j} & 1 \leq j \leq d^* \\ \frac{\tilde{a}_{i,j} - (1 - c_j) \tilde{a}'_{i,j-1}}{c_j} & d^* < j < d^* + 3 \\ \tilde{a}_{i,j+1} & d^* + 3 \leq j \leq K + 3 \end{cases}$$

where  $c_j = \frac{r_{d^*} - r_{j-4}}{r_{j-1} - r_{j-4}}$ . The parameters in  $\tilde{\delta}$  and  $\tilde{\Gamma}$  remain unaltered in this move. We note the difference between our birth and death proposals to those in Sharef et al. (2010) (see equation 3.1 therein), who propose a parameterization where the transformation acts on the exponentials of the spline coefficients. Such a scheme is problematic as the proposed parameters from the death step are not guaranteed to be positive.

## 4 Model selection

In principle we could perform model selection in a formal Bayesian framework via an additional reversible jump or a product space search algorithm (e.g. Carlin and Chib

(1995)). However, in the HMM setting efficient and computationally practical algorithms are very difficult to design due to the potentially large parameter space. Instead, we consider a simple parallel approach where the RJMCMC sampling is performed independently and simultaneously for each candidate model. Based on the sampling outputs, approximate posterior model probabilities, of the form defined in Congdon (2006), and/or the observed likelihood DIC, of the form defined in Chan and Grant (2016), can be computed to guide selection of  $N$ . More specifically, let  $M$  denote the maximum number of states and let  $\theta = (\theta_1, \dots, \theta_M)$ , where each  $\theta_i$  is the parameter set of a spline-based HMM with state space  $\{1, \dots, i\}$ . Let  $\theta^{(i)} = (\theta_1^{(i)}, \dots, \theta_M^{(i)})$ ,  $i = 1, \dots, T$ , represent the  $i$ -th parallel draw from  $f(\theta_k|y^{(n)})$ ,  $k = 1, \dots, M$ . With the simplifying assumptions that (i)  $f(y^{(n)}|\theta, N = k) = f(y^{(n)}|\theta_k, N = k)$ , (ii)  $f(\theta|N = k) = \prod_{i=1}^M f(\theta_i|N = k)$  and (iii)  $f(\theta_{j \neq k}|N = k) \propto \text{constant}$ , a Monte Carlo estimate of  $P(N|y^{(n)})$  may be obtained by the ensemble average (Congdon (2006))

$$\hat{P}(N = k|y^{(n)}) = \frac{1}{T} \sum_{i=1}^T P(N = k|y^{(n)}, \theta^{(i)}), \quad (6)$$

where  $P(N = k|y^{(n)}, \theta^{(i)}) = \frac{f(y^{(n)}|\theta_k^{(i)}, N=k)f(\theta_k^{(i)}|N=k)P(N=k)}{\sum_{k=1}^M f(y^{(n)}|\theta_k^{(i)}, N=k)f(\theta_k^{(i)}|N=k)P(N=k)}$ . Note that since we are not directly sampling over the joint posterior  $P(\theta|y^{(n)})$ , the estimator given in (6) is no longer unbiased (see Robert et al. (2008)). However, it was confirmed to be accurate enough in our simulation experiments and other studies made similar experiences (see Chen et al. (2011) for examples in the context of multiple-regime financial time series models). The DIC criterion is defined as

$$DIC(m) = \mathbf{E}_{\theta_m}[D(\theta_m)|y^{(n)}] + P_D(m), \quad (7)$$

where  $D(\theta_m) = -2 \log(f(y^{(n)}|\theta_m))$  is the deviance for model  $m$ ,  $P_D(m) = \mathbf{E}_{\theta_m}[D(\theta_m)|y^{(n)}] - D(\hat{\theta}_m)$  is a measure of effective number of parameters and  $\hat{\theta}_m$  is the posterior mode of  $\theta_m$ . A sample-based approximation of (7) is obtained as

$$\widehat{DIC}(m) = -\frac{4}{T} \sum_{i=1}^T \log(f(y^{(n)}|\theta_m^{(i)})) + 2 \log(f(y^{(n)}|\hat{\theta}_m)),$$

where  $\hat{\theta}_m = \operatorname{argmax}_{\theta_m^{(i)}: i=1 \dots T} f(y^{(n)}|\theta_m^{(i)})f(\theta_m^{(i)})$ . The model with the lowest  $\widehat{DIC}$  is favoured. In our simulation study described below we find that it performs less well than the estimator

based on (6).

## 5 Simulation studies

### 5.1 Description of experiments

We conduct three simulation experiments to examine the feasibility of the proposed methodology and to compare with two other nonparametric HMM inference methods, namely the frequentist spline-based approach of Langrock et al. (2015) (Models 1 and 2) and the Bayesian nonparametric approach of Yau et al. (2011) (Model 3). For Model 1 we consider the 2-state HMM (see top panel of Figure 1) of Langrock et al. (2015) with emission distributions

$$y_t|x_t = 1 \sim \mathcal{N}(-15, 11^2),$$

$$y_t|x_t = 2 \sim 0.35\mathcal{N}(-5, 9^2) + 0.65\mathcal{N}(30, 10^2),$$

where the transition probabilities are set to  $\gamma_{1,2} = \gamma_{2,1} = 0.1$  and  $n = 800$ . For Model 2, we consider a 3-state HMM with a unimodal positively skewed emission in state 1, a bimodal distribution in state 2, and a unimodal negatively skewed distribution in state 3 (see middle panel of Figure 1). We use B-splines to construct these densities and the details of the spline parameters are omitted here (R-code provided in Appendix). The states of the underlying Markov chain were generated using  $\delta = (1/3, 1/3, 1/3)$ ,  $\gamma_{11} = \gamma_{22} = \gamma_{33} = 0.85$ ,  $\gamma_{2,1} = \gamma_{2,3} = 0.075$ ,  $\gamma_{1,2} = \gamma_{3,2} = 0.1$  and  $\gamma_{1,3} = \gamma_{3,1} = 0.05$ , from which  $n = 1500$  observations were simulated from the corresponding emission distribution using the inverse transform sampling scheme (Devroye, 1986). Model 3 is a 2-state HMM considered in Yau et al. (2011) (the *trimod* case) with emissions specified as a mixture of three well-separated normal distributions (see bottom panel of Figure 1):

$$y_t|x_t = 1 \sim \frac{1}{3}\mathcal{N}(-4, 1) + \frac{1}{3}\mathcal{N}(0, 1) + \frac{1}{3}\mathcal{N}(8, 1),$$

$$y_t|x_t = 2 \sim \frac{1}{3}\mathcal{N}(-3, 1) + \frac{1}{3}\mathcal{N}(1, 1) + \frac{1}{3}\mathcal{N}(9, 1),$$

and  $\gamma_{1,2} = \gamma_{2,1} = 0.05$ . For this model we consider data sets of length  $n = 1000$  and  $5000$ . In all simulation scenarios, the number or the structure of the emission distributions are

hidden from the empirical marginal distributions, with Model 3 posing the most serious challenges even when  $N = 2$  is assumed to be known. We shall use Models 1 and 2 to assess our method on selecting the correct number of states and recovering the emission densities, while for Model 3 we will focus on inference on the transition dynamics of the hidden Markov chain with the same settings as in Yau et al. (2011) with  $N = 2$  pre-fixed and  $\gamma_{1,2} = \gamma_{2,1} = \rho$  known a-priori.

## 5.2 Estimation procedure and results

We present results for each simulation model based on 10 independent MCMC runs, one for each replicate of the simulated data set. We fixed hyperparameters of the parameter priors at  $\epsilon_1 = \epsilon_2 = 1$  while the settings for other unspecified constants are given in Table 1 of the Appendix. For Models 1 and 2 we implement the parallel sampling in each repetition where we place a uniform prior on  $N$  over the candidate set  $\{2, 3, 4, 5\}$ . Our posterior samples for each value of  $N$  are based on 50k iterations of the proposed sampler after a burn-in of 50k iterations. For inference in Model 3 we incorporate the information that both states have a mean level close to zero in our initialization stage. This corresponds to the assumptions made in Yau et al. (2011) that  $m_1 = 0$  and  $m_2 \sim \mathcal{N}(0, 1)$  to avoid excessive times to converge. Our algorithm is run for 150k iterations, with the first 100k iterations discarded as burn-in. We monitored the parameters as well as the likelihood of the models generated by the Markov chain and found that the chosen burn-in periods are generally sufficient to obtain reliable results. Further details regarding the performance of the MCMC algorithm are discussed in the Appendix. On a PC computer having CORE i7 - 6700 CPU, at 3.4 GHz and 16 GB RAM, the average computational time for generating 10k MCMC samples for Models 1 ( $N=2$ ), 2 ( $N=3$ ) and 3 ( $n=1000$ ) using the R programming language was about 110, 200 and 120 seconds, respectively. To facilitate demonstration and comparison, a single HMM was fitted to each simulated data set based on the posterior means of model parameters  $R_{\hat{K}}$ ,  $A_{\hat{K}}$ ,  $\delta$  and  $\Gamma$  (after post-processing the posterior samples following the procedures outlined in the Appendix).

For Model 1, the correct number of states ( $N = 2$ ) is identified in all repetitions by

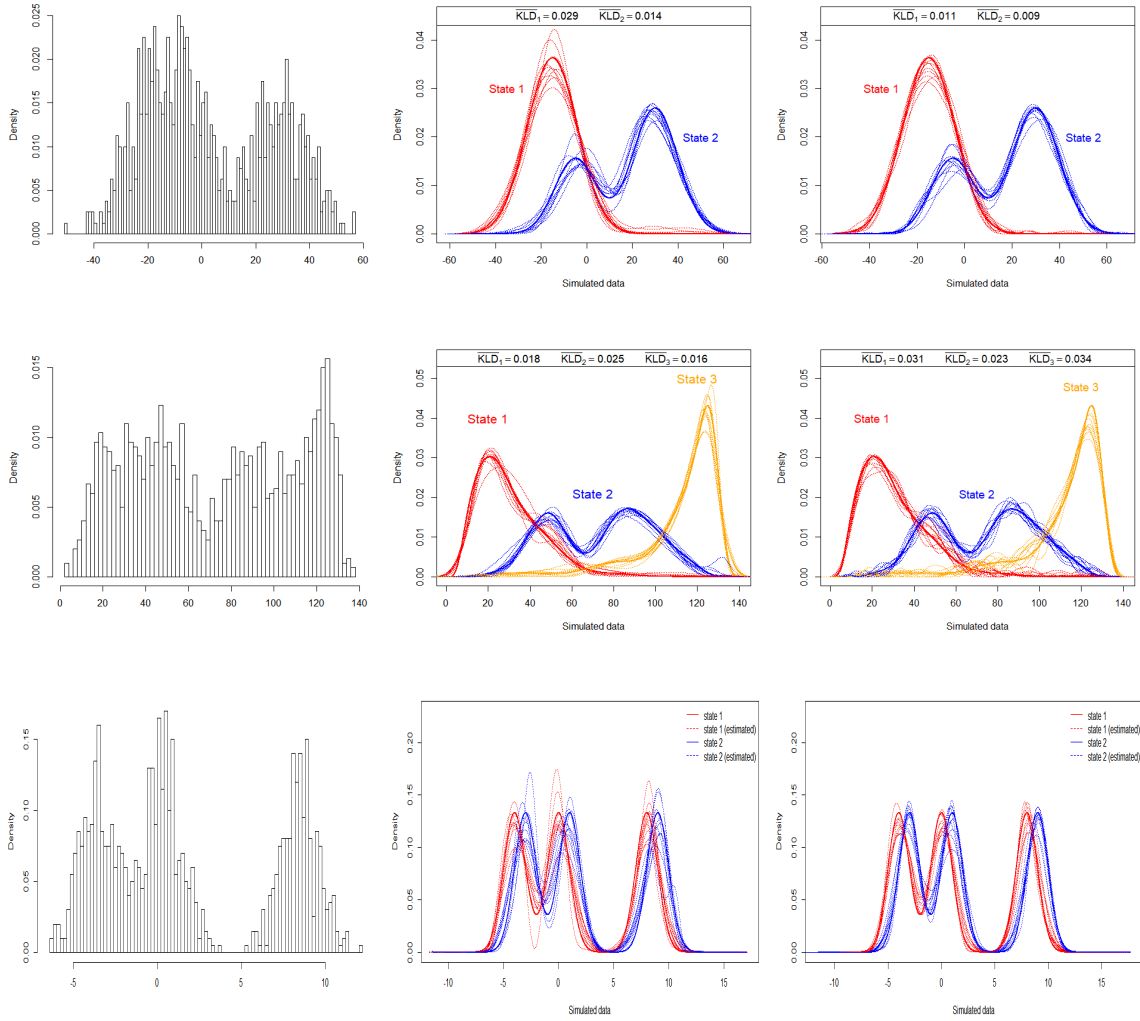


Figure 1: Results for simulation Model 1 (top row), 2 (middle row) and 3 (bottom row). Left column (top and middle): marginal histogram of a data set simulated from the true model; middle column (top and middle): true (solid curves) and estimated (dashed curves) densities of the emission distributions obtained in each replication using our method, with average Kullback–Leibler divergences (KLDs) for state  $i$  ( $\overline{KLD}_i$ ) indicated on the top; right column (top and middle): true (solid curves) and estimated (dashed curves) densities of the emission distributions obtained in each replication using the Langrock et al.’s method, with the average KLDs indicated on the top. Bottom row: marginal histogram of a data set ( $n = 1000$ ) simulated from the model (left), true and estimated densities of the emission distribution obtained in each replication when  $n = 1000$  (middle) and those obtained in each replication when  $n = 5000$  (right).

our Monte Carlo estimator of (6), with averaged posterior probability of  $\hat{P}(N = 2|y^{(n)})$  equal to one (rounded to 3 decimal places). The DIC, however, selected  $N = 2$  only in 50% of the cases favouring a larger  $N$  otherwise. Conditional on  $N = 2$ ,  $K = 6$  (i.e. 10 basis elements) or 7 are suggested as the posterior mode with a frequency of 40% and 60%, respectively. Figure 1 (top row middle panel) shows the true as well as estimated emission densities obtained in the 10 repetitions and these agree reasonably well in general. This is to be compared with Langrock et al.’s (2015) method of using 31 basis elements for the estimation (see top row right panel of Figure 1). We can see that our fitted models are considerably more parsimonious but still achieve comparable density fits in terms of the average Kullback-Leibler divergences (KLDs) between the estimated and true emission densities. There were virtually no differences in the decoding of the state sequence via the Viterbi algorithm, where Langrock et al.’s and our methods yielded similar proportion of correctly classified observations of 93.3% and 93.5% (averaged over the 10 repetitions), respectively.

For Model 2, we obtained  $\hat{P}(N = 3|y^{(n)}) = 1$  in all replicates. The DIC only selected the true model in 6 out of 10 simulation runs and favoured, again, a larger  $N$  in the remaining runs. With  $N = 3$ ,  $K = 9$  or 10 are suggested as the posterior mode with a frequency of 40% and 50%, respectively. In all 10 repetitions our algorithm gives reasonable appearing estimates for the emission (see row 2 middle panel of Figure 1). In order to compare with Langrock et al. (2015), we also followed their estimation approach to fit a B-spline HMM in each repetition, where we set  $K = 43$  and smoothing parameter  $\lambda = (2800, 1600, 2400)$  based on limited experiments of our own and a grid search for  $\lambda$  on  $\{800, 1200, 1600, 2000, 2400, 2800, 3200, 3600\}^3$ . From Figure 1 (middle row right panel) we can see that their approach, due to the assumption of global smoothing parameters, has difficulty in modelling densities that are subject to a varying degree of smoothness over the domain. Despite the fact that a much larger number of basis elements has been used, their method leads to larger average KLDs for emission distributions in state 1 and 3, compared to our fits. The average decoding accuracy over the 10 replicates is 89.8% and 88.7% for models estimated using our and their method.

For Model 3 with  $n = 1000$ ,  $K = 14$  is suggested by the algorithm in 90% of the simulation runs. Figure 1 (bottom row middle panel) shows the true and estimated emission densities obtained in each replication. Despite the relatively small data size and the vague prior information, the tri-modal nature of the emission distributions is successfully identified in all replicates with our method. The average posterior means ( $\pm 1$  standard deviation) of the transition probability  $\rho$  is 0.08 ( $\pm 0.032$ ), which is consistent with the true value  $\rho = 0.05$ . When  $n$  is increased to 5000,  $K = 15$  is suggested in 70% of the replicates. The estimated emission densities along with the true ones are displayed in the bottom row right panel of Figure 1, and the posterior estimates of  $\rho$  is now 0.055 ( $\pm 0.005$ ). As expected, an increase in data size improves the estimation accuracy and reduces uncertainty. When comparing these results with those reported in Table 2 (cases when  $T=1000$  and 5000) of Yau et al. (2011), it seems that our method achieves comparable and slightly better performance in the case when  $n = 1000$  and 5000, respectively. It should also be pointed out that Langrock et al.’s method suffered significantly from numerical issues in this scenario. Even with careful selection of initial parameter values and smoothing parameters, it failed to converge or find a solution in over 40% of the simulation runs.

## 6 Applications

### 6.1 Oceanic whitetip shark acceleration data

HMMs are very suited to modelling animal movement metrics to study the dynamic patterns of an animal’s behavioural states (e.g., resting, foraging or travelling) in ecology (Patterson et al., 2009; Langrock et al., 2012, 2018). We consider the overall dynamic body acceleration (ODBA) collected from an oceanic whitetip shark at a rate of 16 Hz over 24 hours noting that a larger replicate data set was analyzed in Langrock et al. (2018). The raw ODBA values are averaged over 15 sec non-overlapping windows and log transformed (IODBA), resulting in 5760 observations. The marginal distribution of the transformed data is illustrated in Figure 2. We first model the IODBA values using a B-spline HMM with  $N$  fixed to three states as in Langrock et al. (2018). The hyperparameters of the prior

distributions are specified as  $\epsilon_1 = \epsilon_2 = 1$ ,  $a = -5.5$  and  $b = -1$ . We set  $\tau_1 = 0.07$ ,  $\tau_2 = 0.1$ ,  $\tau_3 = 0.5$ ,  $\tau_4 = 1.6$ ,  $\tau_5 = 0.14$  and  $\alpha = 1.8$  with the help of a few pilot runs. Our posterior inference was based on 25k sweeps of the RJMCMC algorithm after a burn-in of 25k sweeps. The sampling process took about 50 minutes in R (for the same hardware specs as above). The posterior modal number of knots is 10, with  $\hat{P}(K = 10|data) = 0.952$ . The estimated emission densities are shown in Figure 2 (left panel), where the knots and spline coefficients are set to their posterior averages, conditioned on  $K = 10$ . As was pointed out in Langrock et al. (2018), there could be a potential lack of fit if one chooses to model the emission distributions by some common parametric family. For comparison, we also fitted a B-spline HMM using Langrock et al.’s (2015) method. The resulting density estimates are shown in Figure 2 (right panel). Here we have set  $K = 39$  to ensure enough flexibility and selected  $\lambda = (300, 1, 400)$  for the smoothing parameters based on our experiments. The resulting 3-state HMM has more than 120 parameters, for which we experienced numerical stability issues in the process of the smoothing parameter selection. In contrast, our approach used no more than 60 parameters while achieving comparable density fits, with some improvement in capturing the spikiness of the emission of the middle state. Note that we also obtained posterior uncertainties for the parameters at no extra computational cost. To verify if these data support a model with  $N = 3$  fixed we performed model selection using (6) assuming a discrete uniform prior for  $N$  over  $\{2, \dots, 8\}$ . Interestingly, we found a posterior mode at  $N = 7$  with probability one, thus strongly indicating that the data support a considerably larger number of states than originally assumed in Langrock et al. (2018) (more details are provided in the appendix).

## 6.2 A conditional HMM to study movement in sleep

Sleep is strongly affecting a person’s physical and mental well-being and plays a key role in adverse health conditions such as, for example, diabetes, cardiovascular disease and depression (Foster, 2020). Monitoring sleep could be essential to gaining insight into a subject’s circadian rhythm and health status. The gold standard for measuring sleep is laboratory based polysomnography (PSG) but due to the high cost and intrusiveness of



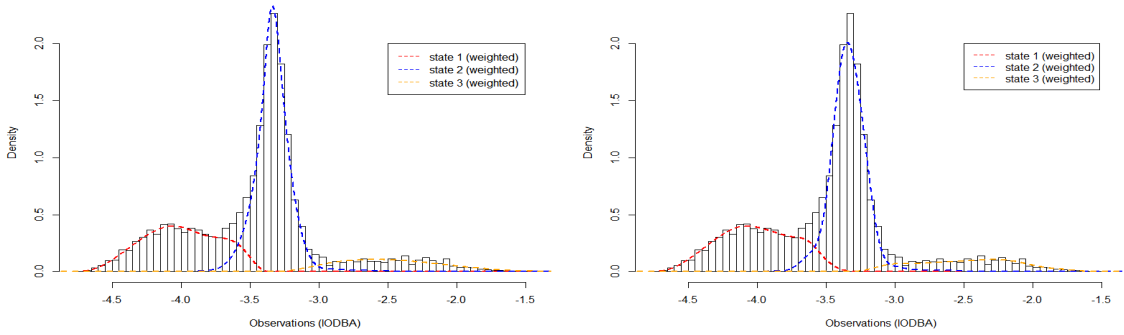


Figure 2: Histogram of 15s-averaged IODBA values along with the estimated emission densities (weighted according to their proportion in the stationary distribution of the estimated Markov chain) obtained from our method (left panel) and Langrock et al’s method (right panel).

laboratory settings, PSG is of limited use to investigate daily sleep rhythms in practice. Instead, actigraphy has become increasingly popular in sleep research due to the wide availability of low-cost devices that can be fixed to the body in non-obtrusive ways to obtain objective recordings of rest-activity rhythms over long periods of time for a subject living in their own environment (Ancoli-Israel et al., 2003; Huang et al., 2018; Winnebeck et al., 2018). Statistical methods for analysing accelerometer data, such as functional data analysis and HMM based methods, mainly focused on studying physical activity and/or the sleep-wake cycle of a subject, but so far little attention has been paid to analysing the sleep periods (see Xiao et al. (2014); Huang et al. (2018); Li et al. (2020) and references therein). Recently, Winnebeck et al. (2018) demonstrated the potential of accelerometer recordings taken at the wrist for extracting basic periodic patterns of sleep physiology by analyzing the *“Locomotor Inactivity During Sleep”* (LIDS), a simple ad-hoc inverse transformation of the physical activity (PA) data which enhances non-movement during sleep. They found that LIDS oscillate in phase with markers of *“deeper”* sleep, and out of phase with markers of *“lighter”* sleep as well as rapid eye movement (REM) sleep. While their findings are very promising, their approach did not allow them to systematically quantify the sleep periods or analyse the stochastic dynamics of the sleep process on an individual basis.

Assuming that sleep periods are contained within State 1, e.g. the state that is associated with the lowest activity level, we extend our model above, referred to as "main-HMM", by inserting a second or "sub-HMM" that is invoked conditional on State 1 of the main HMM. Bayesian inference thus proceeds in two steps to retrospectively (i) characterize the sleep-wake patterns in the entire activity data set by means of estimating the main- HMM and (ii) further identify states of the small movements and/or absence of activity in State 1 by means of a sub-HMM conditional on State 1. The extension of such an approach over the one by Winnebeck et al. (2018) will be that, firstly, it gives a principled stochastic model from which we can systematically estimate many important parameters that characterize an individual's sleep-wake cycle, such as duration and center of rest times, amount and regularity of activity etc. (see Huang et al. (2018) ) and, secondly, it allows us to model the individual stochastic dynamics of the rest state activity which does not appear strictly periodic as seen on the aggregate level in Winnebeck et al. (2018). By conditioning on the rest state alone there is no need to apply any ad-hoc transformation and also our likelihood for the sub-model will not be influenced by the relatively large values and variability of the activity observed during the day.

The number of states  $N$  of the main HMM may be estimated by parallel sampling as described in section 4. For the sub-HMM we assume 2 sub-states, 1.1 and 1.2, of State 1 to potentially capture the ultradian oscillations between higher and lower intensity of movement during sleep such as identified by Winnebeck et al. (2018) who alluded to the possibility that these oscillations might be due to the ca 120 min periodic transitions between the Non-REM and REM stages of sleep. Accelerometer measurements often are discrete valued variables associated with counting the threshold crossing of movement intensity. To take account of the large number of zeros typically observed during a rest or sleep state, we assume a zero inflation of the emission distributions at both HMM levels

$$f_{x_t}(y_t) = w_{x_t} \delta_0 + (1 - w_{x_t}) f_{x_t}^B(y_t), \quad (9)$$

where  $x_t$  indicates the underlying state at time  $t$ ,  $w_{x_t}$  represents the state-specific zero weight such that  $0 \leq w_{x_t} \leq 1$ ,  $\delta_0$  is the Dirac delta distribution and  $f_{x_t}^B(y_t)$  is defined in (1). Following Gassiat et al. (2016a) we can establish identifiability of the resulting

HMM provided that at most one  $w_{x_t}$  is equal to one and that  $\{\delta_0, f_1^B, \dots, f_N^B\}$  are linearly independent. In our analysis these conditions are always satisfied. Posterior inference for the resulting hierarchical model may be achieved by sequentially sampling from  $f(\Theta_1|\{y_t\})$  and  $f(\Theta_2|\{y_t\})$ , where  $\Theta_1$  and  $\Theta_2$  represent the parameter sets of the main and the sub-HMM, respectively. The MCMC methodology described in section 3 can be used to simulate from  $f(\Theta_1|\{y_t\})$ . An additional MH step is needed to update the  $w_i$ , in a manner that is similar to that for  $\delta$ . For the sub-HMM we assume that

$$f(\Theta_2|\{y_t\}) = \int f(\Theta_2|V, \{y_t\})f(V|\{y_t\})dV$$

where  $V = V(\{y_t\}, \Theta_1)$  is the Viterbi-decoded state sequence obtained from the main HMM. To simulate from  $f(\Theta_2|\{y_t\})$  we first generate posterior samples of  $V$  by plugging in posterior samples of  $\Theta_1$  into  $V(\cdot)$ , and then simulate from  $f(\Theta_2|V, \{y_t\})$  following the same MCMC procedures as used for the main-HMM. Note that the likelihood  $f(\{y_t\}|\Theta_1)$  and  $f(\{y_t\}|V, \Theta_2)$  can be evaluated via (2). When computing the latter, data in  $V$  that were assigned to the higher active states 2 or 3, are treated as "missing" (Zucchini et al., 2016). Mathematically this corresponds to replacing the diagonal matrices  $P(\cdot)$  in (2) by the identity matrix for the associated time points.

We analyse a data set ("subject 9") from a wrist-watch accelerometer available in Huang et al. (2018) with measurements per minute over 4 days. To save computational time inference for the main-HMM is based on the raw PA data averaged over 5-min as in Huang et al. (2018). Parallel sampling was performed for  $N = \{2, 3, 4, 5\}$  for 100k iterations, of which 50k were discarded as burn-in. The number of states for the main HMM was thus estimated as 3, with posterior probability of 0.706. This is in agreement with Huang et al. (2018) who generally used  $N = 3$  to analyze more than 40 subjects' PA data using a parametric Gaussian HMM but also reported that model selection for the individual data sets was challenging as their inference algorithm failed to converge for increasing  $N$ . Setting  $N = 3$ , Figure 3 (top panel) depicts the 5-min averaged PA data along with the Viterbi-decoded states and, in the panel underneath, the cumulative probabilities of the three states at each time point conditioned on the set of all observations. It is apparent that State 1 is characterized by relatively long periods of low PA at night time. Other states

(in pink and red shades) usually correspond to day-time activities of varying intensity which will depend on the subject’s lifestyle, but also to potential interruptions of sleep such as in the second night of the subject. The main-HMM suggests that the subject had a regular sleep time with no or very few sleep disruptions during the monitoring period. Our posterior simulation for the sub-HMM is based on realisations of  $V$  obtained from the last 50k MCMC samples of  $\Theta_1$  and to be able to better focus on the detail of activity during sleep we use the higher resolution 1-min PA data. Results presented are based on a single sub-HMM conditioned on the posterior point estimates of the model parameters. Figure 3 (panels (1)-(4)) shows the Viterbi-decoded time series of the 1-min PA data for each night along with the cumulative probability of the two sub-states at each time point. State 1.1 is characterized by a large probability of observing zero, with posterior mean  $\hat{w}_1$  of 0.898 while State 1.2 corresponds to a moderately higher level of activity with posterior mean  $\hat{w}_2$  of 0.246. We found in a separate analysis - not reported here - that the occurrence of State 1.2 often coincides with a change in body position which was recorded at the same time by a chest sensor. Regarding the findings of Winnebeck et al. (2018) and with the due note of care that small or no activity is not synonymous to sleep, we hypothesize that, sub-state 1.2 might be associated with REM and also lighter sleep stages as well as possible disruptions into wake. The graphs clearly show that for a single subject the transitions between and the times spent in the sub-states are subject to stochasticity. An analysis of the estimated parameters, in particular the transition probabilities of the fitted sub-HMM will provide a systematic quantitative summary which could be used, for example, to compare sleep behaviour between subjects. For our example subject the posterior means ( $\pm 1$  standard deviation) of the diagonal entries of  $\Gamma$  are  $\hat{\gamma}_{1.1,1.1} = 0.963 (\pm 0.01)$  and  $\hat{\gamma}_{1.2,1.2} = 0.889 (\pm 0.023)$ . A lower value of  $\hat{\gamma}_{1.1,1.1}$  and/or higher value of  $\hat{\gamma}_{1.2,1.2}$  means that the subject has a higher probability of leaving state 1.1 and/or a larger expected staying time in state 1.2 which may be associated with poorer sleep quality during the monitoring period. The decoding results for the sub-HMM further allow us to investigate the variation within and between courses of a sleep bout. For instance, it appears that our subject may be finding it more difficult to fall asleep as they experienced lighter sleep and/or interruptions towards

the start of their sleep bout. We note that these are detailed patterns that allow us to focus on studying rest or sleep periods which are not discernible from the main-HMM. The hierarchical modelling approach by means of a conditional HMM is also justified noting that an unconditional HMM with number of states fixed to four is rarely likely to assign two sleep-related states as for most subjects the higher values and variability of day-time activity will dominate the likelihood and the assignment of states.

## 7 Summary and further Discussion

In comparison to other nonparametric approaches the spline-based HMM approach is attractive because of its simplicity in model interpretation. Here we propose and develop a Bayesian methodology for inference in B-spline-based HMMs where the number of hidden states  $N$  may be unknown along with all other model parameters. With  $N$  fixed, we introduce a RJMCMC algorithm that allows for a parsimonious and efficient positioning of the spline knots as we were able to demonstrate in simulations and case studies. It further appears that the implied computational efficiency allows us to realistically conduct model selection on  $N$  which is a notoriously difficult problem due to challenging convergence problems even in - or perhaps because of - parametric approaches and when dealing with more states and larger data sets. Here we propose to follow a straightforward parallel sampling scheme, where quantities like posterior model probability or the DIC can be estimated. Our simulation studies demonstrate the resulting effectiveness of the posterior probability estimator of (6) in selecting the correct model, which compared favourably over the DIC.

We believe that within the spline-based modelling framework, a Bayesian inference method is attractive compared to the frequentist approach introduced in Langrock et al. (2015), not only because we circumvent the challenging problems they face, such as the selection of smoothing parameters and the quantification of uncertainty on model parameters, but also because it allows for more stable and also more parsimonious estimation of the emission densities while achieving comparable or even slightly better performance. Langrock et al. (2018) didn't approach model selection on  $N$  but we were able to estimate a B-spline based HMM where  $N$  could be, and was indeed estimated to be, consider-

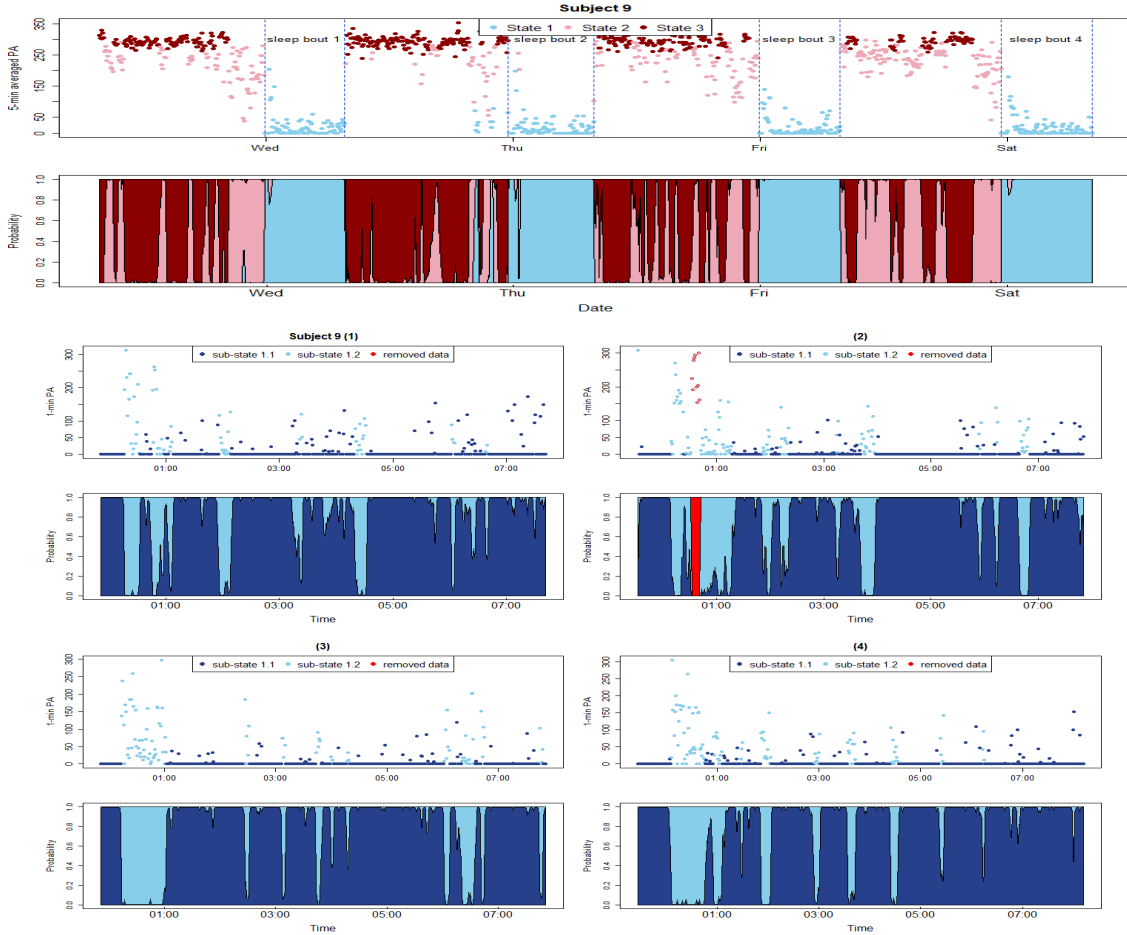


Figure 3: Results for subject 9. Top row upper panel: 5-min averaged PA data over a monitoring period of 4 days, where colour indicates the Viterbi-decoded state at each time under the estimated main HMM and the dashed lines indicate the start and end time of each identified sleep bouts (the onset of a sleep bout was set to the first time the Viterbi-decoded states enters state 1 and stayed in that state for longer than 30 minutes, while the end of a sleep bout was taken to be the time point at which the Markov chain leaves state 1 and stays for over 30 minutes in any of the other states); top row lower panel: the cumulative posterior probability of the state at each time under the estimated outer model (i.e.  $P(x_t \leq i | \hat{\Theta}_1, \{y_t\}); i = 1, 2, 3$ ). Middle and bottom rows (panels (1)-(4)) display 1-min PA data with colours indicating the Viterbi-decoded state at each time (top) and the corresponding cumulative probability of each sub-state at each time (bottom) for sleep bouts 1-4 identified from the outer model, respectively. Removed data (in red) are those that are assigned to a more active state instead of state 1 by the fitted outer-HMM.

ably higher for the same kind of animal movement data. This comparison highlights the advantages gained from being able to address model selection on  $N$  and the use of a non-parametric approach for explorative data analysis. An interesting further question would be whether the 3-state nonparametric model can be replaced by a 7-state parametric approach, assuming for instance a mixture of Gaussian emission densities, which can capture a higher degree of multimodality in the marginal distribution. Our approach also compares favourably with the Bayesian nonparametric model developed in Yau et al. (2011) as it possesses a relatively simple model formulation and the ability to address the case where  $N$  is unknown. Finally, the application to sleep research highlights the flexibility of our Bayesian modelling approach that can be extended in a relatively straightforward way to hierarchical scenarios such as the conditional HMM. The extension to a hierarchical framework of a sub-HMM within an overall HMM here allows us to focus directly on PA during sleep times and to quantify in a systematic way an individual’s stochastic dynamic behaviour of transitions between, and sojourn times within, sub-states that may be associated with deeper and lighter or interrupted sleep stages. This is an important area of interest to sleep and circadian biology research.

The modelling framework may be extended in other ways, with appropriate modifications of the proposed algorithm. For instance, the homogeneous assumption on the hidden Markov chain of our spline-based HMM can be easily relaxed to allow for covariate dependent transition probability matrix. One way to achieve this is to employ the standard multinomial logistic link function for the transition probabilities (Zucchini et al., 2016) so that  $\Gamma$  is parameterized in terms of the covariates and step (e) of the MCMC algorithm needs to be adjusted accordingly. A generalization to a multivariate observation process also is straightforward - at least in principle. In particular, assuming contemporaneous conditional independence, i.e.  $f_{x_t}(y_1, \dots, y_M) = \prod_{i=1}^M f_{x_t,i}(y_i)$ , we can model the state-dependent joint density by assuming univariate B-splines for the corresponding marginal densities. In this case multiple birth and death moves are required for the RJMCMC to update the knot configurations for each component of  $(y_1, \dots, y_M)$  in a deterministic or random manner. However, developing an efficient MCMC methodology for spline-based

HMMs with a more general multivariate distribution is non-trivial and our future research is undertaken in this direction.

## ACKNOWLEDGEMENT

We wish to thank Prof. Roland Langrock, Dr. Yannis Papastamatiou and Dr. Yuuki Watanabe for providing the oceanic whitetip shark data. We wish to acknowledge Dr. Qi Huang and Prof. Francis Lévi for their support on the analysis of the human accelerometer data. We would also like to acknowledge the Warwick Statistics Department for the continued support of Sida Chen during his PhD research.

## References

- Alexandrovich, G., Holzmann, H., and Leister, A. (2016). Nonparametric identification and maximum likelihood estimation for hidden Markov models. *Biometrika*, 103(2):423–434.
- Ancoli-Israel, S., Cole, R., Alessi, C., Chambers, M., Moorcroft, W., and Pollak, C. P. (2003). The role of actigraphy in the study of sleep and circadian rhythms. *Sleep*, 26(3):342–392.
- Billier, C. (2000). Adaptive bayesian regression splines in semiparametric generalized linear models. *Journal of Computational and Graphical Statistics*, 9(1):122–140.
- Cappé, O., Moulines, E., and Rydén, T. (2005). *Inference in Hidden Markov Models*. Springer-Verlag New York.
- Cappé, O., Robert, C. P., and Rydén, T. (2003). Reversible jump, birth-and-death and more general continuous time Markov chain Monte Carlo samplers. *Journal of the Royal Statistical Society: Series B (Statistical Methodology)*, 65(3):679–700.
- Carlin, B. P. and Chib, S. (1995). Bayesian model choice via Markov chain Monte Carlo methods. *Journal of the Royal Statistical Society: Series B (Methodological)*, 57(3):473–484.



- Celeux, G. and Durand, J.-B. (2008). Selecting hidden Markov model state number with cross-validated likelihood. *Computational Statistics*, 23(4):541–564.
- Chan, J. C. and Grant, A. L. (2016). Fast computation of the deviance information criterion for latent variable models. *Computational Statistics & Data Analysis*, 100:847–859.
- Chen, C. W., Gerlach, R. H., and Lin, A. M. (2011). Multi-regime nonlinear capital asset pricing models. *Quantitative Finance*, 11(9):1421–1438.
- Congdon, P. (2006). Bayesian model choice based on Monte Carlo estimates of posterior model probabilities. *Computational statistics & data analysis*, 50(2):346–357.
- De Boor, C. (2001). *A practical guide to splines*. Springer, New York.
- De Castro, Y., Gassiat, E., and Le Corff, S. (2017). Consistent estimation of the filtering and marginal smoothing distributions in nonparametric hidden Markov models. *IEEE Transactions on Information Theory*, 63(8):4758–4777.
- Devroye, L. (1986). Sample-based non-uniform random variate generation. In *Proceedings of the 18th conference on Winter simulation*, pages 260–265. ACM.
- DiMatteo, I., Genovese, C. R., and Kass, R. E. (2001). Bayesian curve-fitting with free-knot splines. *Biometrika*, 88(4):1055–1071.
- Foster, R. G. (2020). Sleep, circadian rhythms and health. *Interface Focus*, 10(3):20190098.
- Fox, E. B., Sudderth, E. B., Jordan, M. I., and Willsky, A. S. (2011). A sticky hdp-hmm with application to speaker diarization. *The Annals of Applied Statistics*, pages 1020–1056.
- Friedman, J., Hastie, T., and Tibshirani, R. (2001). *The elements of statistical learning*, volume 1. Springer series in statistics New York.
- Gassiat, É., Cleynen, A., and Robin, S. (2016a). Inference in finite state space non parametric hidden Markov models and applications. *Statistics and Computing*, 26(1-2):61–71.

- Gassiat, E., Rousseau, J., et al. (2016b). Nonparametric finite translation hidden Markov models and extensions. *Bernoulli*, 22(1):193–212.
- Green, P. J. (1995). Reversible jump Markov chain Monte Carlo computation and Bayesian model determination. *Biometrika*, 82(4):711–732.
- Hastie, D. I., Liverani, S., and Richardson, S. (2015). Sampling from Dirichlet process mixture models with unknown concentration parameter: mixing issues in large data implementations. *Statistics and computing*, 25(5):1023–1037.
- Huang, Q., Cohen, D., Komarzynski, S., Li, X.-M., Innominato, P., Lévi, F., and Finkenstädt, B. (2018). Hidden Markov models for monitoring circadian rhythmicity in telemetric activity data. *Journal of The Royal Society Interface*, 15(139):20170885.
- Kang, K., Cai, J., Song, X., and Zhu, H. (2019). Bayesian hidden Markov models for delineating the pathology of alzheimer’s disease. *Statistical methods in medical research*, 28(7):2112–2124.
- Langrock, R., Adam, T., Leos-Barajas, V., Mews, S., Miller, D. L., and Papastamatiou, Y. P. (2018). Spline-based nonparametric inference in general state-switching models. *Statistica Neerlandica*, 72(3):179–200.
- Langrock, R., King, R., Matthiopoulos, J., Thomas, L., Fortin, D., and Morales, J. M. (2012). Flexible and practical modeling of animal telemetry data: hidden Markov models and extensions. *Ecology*, 93(11):2336–2342.
- Langrock, R., Kneib, T., Sohn, A., and DeRuiter, S. L. (2015). Nonparametric inference in hidden Markov models using p-splines. *Biometrics*, 71(2):520–528.
- Lehéricy, L. (2018). State-by-state minimax adaptive estimation for nonparametric hidden Markov models. *The Journal of Machine Learning Research*, 19(1):1432–1477.
- Lehéricy, L. et al. (2019). Consistent order estimation for nonparametric hidden Markov models. *Bernoulli*, 25(1):464–498.

- Li, X., Zhang, Y., Jiang, F., and Zhao, H. (2020). A novel machine learning unsupervised algorithm for sleep/wake identification using actigraphy. *Chronobiology International*, pages 1–14.
- Patterson, T. A., Basson, M., Bravington, M. V., and Gunn, J. S. (2009). Classifying movement behaviour in relation to environmental conditions using hidden Markov models. *Journal of Animal Ecology*, 78(6):1113–1123.
- Piccardi, M. and Pérez, Ó. (2007). Hidden markov models with kernel density estimation of emission probabilities and their use in activity recognition. In *2007 IEEE Conference on Computer Vision and Pattern Recognition*, pages 1–8. IEEE.
- Pohle, J., Langrock, R., van Beest, F. M., and Schmidt, N. M. (2017). Selecting the number of states in hidden Markov models: pragmatic solutions illustrated using animal movement. *Journal of Agricultural, Biological and Environmental Statistics*, 22(3):270–293.
- Rabiner, L. R. (1989). A tutorial on hidden Markov models and selected applications in speech recognition. *Proceedings of the IEEE*, 77(2):257–286.
- Robert, C. P., Marin, J.-M., et al. (2008). On some difficulties with a posterior probability approximation technique. *Bayesian Analysis*, 3(2):427–441.
- Robert, C. P., Ryden, T., and Titterton, D. M. (2000). Bayesian inference in hidden Markov models through the reversible jump Markov chain Monte Carlo method. *Journal of the Royal Statistical Society: Series B (Statistical Methodology)*, 62(1):57–75.
- Sharef, E., Strawderman, R. L., Ruppert, D., Cowen, M., Halasyamani, L., et al. (2010). Bayesian adaptive b-spline estimation in proportional hazards frailty models. *Electronic journal of statistics*, 4:606–642.
- Spiegelhalter, D. J., Best, N. G., Carlin, B. P., and Van Der Linde, A. (2002). Bayesian measures of model complexity and fit. *Journal of the Royal Statistical Society: Series B (Statistical Methodology)*, 64(4):583–639.

- Vernet, E. et al. (2015). Posterior consistency for nonparametric hidden Markov models with finite state space. *Electronic Journal of Statistics*, 9(1):717–752.
- Winnebeck, E. C., Fischer, D., Leise, T., and Roenneberg, T. (2018). Dynamics and ultradian structure of human sleep in real life. *Current Biology*, 28(1):49–59.
- Xiao, L., Huang, L., Schrack, J. A., Ferrucci, L., Zipunnikov, V., and Crainiceanu, C. M. (2014). Quantifying the lifetime circadian rhythm of physical activity: a covariate-dependent functional approach. *Biostatistics*, 16(2):352–367.
- Yau, C., Papaspiliopoulos, O., Roberts, G. O., and Holmes, C. (2011). Bayesian non-parametric hidden Markov models with applications in genomics. *Journal of the Royal Statistical Society: Series B (Statistical Methodology)*, 73(1):37–57.
- Zucchini, W., MacDonald, I. L., and Langrock, R. (2016). *Hidden Markov models for time series: an introduction using R*. Chapman and Hall/CRC.

Appendix to the paper  
**Bayesian inference for spine-based hidden  
Markov models**

Sida Chen and Bärbel Finkenstädt Rand  
Department of Statistics, University of Warwick

## **A Further details of the reversible jump MCMC algorithm**

In this section, we give further computational and implementational details related to the reversible jump MCMC algorithm presented in Section 4 and establish the validity of the algorithm.

### **A.1 Acceptance probabilities for the fixed dimensional moves**

Moves (a) and (b) are standard Metropolis-Hastings updates. For (a), the acceptance probability for relocating the knot  $r_{k^*}$  to the candidate point  $r_c$  is:

$$\min\left(1, \frac{f(y^{(n)}|K, R'_K, \tilde{A}_K, \tilde{\delta}, \tilde{\Gamma})f_{N,[a,b]}(r_{k^*}|r_c, \tau_1^2)}{f(y^{(n)}|K, R_K, \tilde{A}_K, \tilde{\delta}, \tilde{\Gamma})f_{N,[a,b]}(r_c|r_{k^*}, \tau_1^2)}\right),$$

where  $R'_K$  differs from  $R_K$  only in the replacement of  $r_{k^*}$  by  $r_c$ , and  $f_{N,[a,b]}(\cdot|\mu, \sigma^2)$  denotes the density of the truncated normal distribution with mean  $\mu$ , standard deviation  $\sigma$  and bounded on  $[a, b]$ . For move (b) since the proposal is symmetric the acceptance probability is:

$$\min\left(1, \frac{f(y^{(n)}|K, R_K, \tilde{A}'_K, \tilde{\delta}, \tilde{\Gamma})f(\tilde{A}'_K|K, \zeta)}{f(y^{(n)}|K, R_K, \tilde{A}_K, \tilde{\delta}, \tilde{\Gamma})f(\tilde{A}_K|K, \zeta)}\right),$$

where the set of  $\tilde{a}'_{i,j}$  is denoted by  $\tilde{A}'_K$ . In steps (c)-(e) we used log-normal random walk to update the parameters due to the positivity constraint, and the corresponding acceptance probabilities for these moves are, respectively,

$$\min\left(1, \frac{f(\tilde{A}_K|K, \zeta')f(\zeta')\zeta'}{f(\tilde{A}_K|K, \zeta)f(\zeta)\zeta}\right),$$

$$\min\left(1, \frac{f(y^{(n)}|K, R_K, \tilde{A}_K, \tilde{\delta}', \tilde{\Gamma})f(\tilde{\delta}')}{f(y^{(n)}|K, R_K, \tilde{A}_K, \tilde{\delta}, \tilde{\Gamma})f(\tilde{\delta})} \prod_{i=1}^N \frac{\tilde{\delta}'_i}{\tilde{\delta}_i}\right),$$

and

$$\min\left(1, \frac{f(y^{(n)}|K, R_K, \tilde{A}_K, \tilde{\delta}, \tilde{\Gamma}')f(\tilde{\Gamma}')}{f(y^{(n)}|K, R_K, \tilde{A}_K, \tilde{\delta}, \tilde{\Gamma})f(\tilde{\Gamma})} \prod_{i=1}^N \prod_{j=1}^N \frac{\tilde{\gamma}'_{i,j}}{\tilde{\gamma}_{i,j}}\right),$$

where  $\tilde{\delta}'$  and  $\tilde{\Gamma}'$  denote the vectors of proposed  $\tilde{\delta}'_i$  and  $\tilde{\gamma}'_{i,j}$ , respectively.

## A.2 Acceptance probabilities for the birth and death moves

Using the notation of Green (1995), the birth move regarding spline parameters is accepted with probability  $\min(1, A)$ , where A could be expressed in the form

$$\text{likelihood ratio} \times \text{prior ratio} \times \text{proposal ratio} \times \text{Jacobian}.$$

In our context the likelihood ratio is:

$$\frac{f(y^{(n)}|K+1, R_{K+1}, \tilde{A}'_{K+1}, \tilde{\delta}, \tilde{\Gamma})}{f(y^{(n)}|K, R_K, \tilde{A}_K, \tilde{\delta}, \tilde{\Gamma})},$$

where  $\tilde{A}'_{K+1}$  stands for the set of proposed  $\tilde{a}'_{i,j}$  and the likelihood  $f(y^{(n)}|\cdot)$  is given by equation (2). The prior ratio is given by the product of the ratio of the priors on each block of parameters that are involved in this update:

$$\frac{f_U(K+1) \frac{(K+1)!}{(b-a)^{K+1}} \prod_{i=1}^N \prod_{j=1}^{K+5} f_{LG}(\tilde{a}'_{i,j}|\zeta, 1)}{f_U(K) \frac{K!}{(b-a)^K} \prod_{i=1}^N \prod_{j=1}^{K+4} f_{LG}(\tilde{a}_{i,j}|\zeta, 1)}$$

where  $f_U(\cdot)$  denotes the probability mass function of a uniformly distributed random variable on  $\{2, \dots, K_{\max}\}$  and  $f_{LG}(\cdot|\zeta, 1)$  stands for the log-gamma density with shape parameter  $\zeta$  and rate parameter 1. The proposal ratio is given by

$$\frac{d_{K+1}}{(K+1)} \left\{ b_K \frac{\sum_{i=1}^K f_{N,[a,b]}(r_c|r_i, \tau(R_K, i)^2)}{K} \right\}^{-1},$$

where  $f_{N,[a,b]}(\cdot|\mu, \sigma^2)$  denotes the density of a truncated normal distribution with mean  $\mu$ , standard deviation  $\sigma$  and bounded on  $[a, b]$ . Lastly, the Jacobian corresponding to the transformation from  $(R_K, \tilde{A}_K, \tilde{\delta}, \tilde{\Gamma}, r_c, u_1, \dots, u_N)$  to  $(R_{K+1}, \tilde{A}'_{K+1}, \tilde{\delta}, \tilde{\Gamma})$  is

$$|(r_{n^*+2}r_{n^*+3})^N \prod_{i=1}^N (\tilde{a}_{i,n^*+4} - \tilde{a}_{i,n^*+3})|.$$

After simplification  $A$  is thus given by

$$A = \frac{f(y^{(n)}|K+1, R_{K+1}, \tilde{A}'_{K+1}, \tilde{\delta}, \tilde{\Gamma})}{f(y^{(n)}|K, R_K, \tilde{A}_K, \tilde{\delta}, \tilde{\Gamma})} \frac{1}{(b-a)} \frac{\prod_{i=1}^N \prod_{j=n^*+2}^{n^*+4} f_{LG}(\tilde{a}'_{i,j}|\zeta, 1)}{\prod_{i=1}^N \prod_{j=n^*+2}^{n^*+3} f_{LG}(\tilde{a}_{i,j}|\zeta, 1)} \\ \times \frac{d_{K+1}}{b_K} \left\{ \frac{\sum_{i=1}^K f_{N,[a,b]}(r_c|r_i, \tau(R_K, i)^2)}{K} \right\}^{-1} |(r_{n^*+2}r_{n^*+3})^N \prod_{i=1}^N (\tilde{a}_{i,n^*+4} - \tilde{a}_{i,n^*+3})|.$$

Since the birth and death moves are defined in a symmetric way, the acceptance probability for this death move is  $\min(1, A^{-1})$ , where  $K$  is replaced by  $K-1$  and  $n^* = d^* - 1$ .

### A.3 Validity of the algorithm

The validity of the proposed reversible jump MCMC algorithm can be established following standard results in Tierney (1994) and Robert and Casella (2013). First note that the Markov transition kernel for each of the move steps admits the target posterior distribution,  $f$  (defined through equation (3)), as invariant distribution, so a concatenation of these kernels also admits  $f$  as invariant distribution. Irreducibility of the constructed chain can be deduced as the chain can move from one value of  $K$  to any other possible value by increasing or decreasing its value by one at a time, with positive probability. In steps (b), (d) and (e) the proposal density is positive on the natural parameter space and the same holds true for step (a) if we consider several consecutive sweeps. The chain is also aperiodic as there is a strictly positive probability that the chain remains in a neighbourhood of the current state after one sweep of the MCMC procedure. With the above properties the chain is guaranteed to converge to the posterior distribution from almost all initial states (except for a set of posterior probability zero). To replace "almost all" by "all" we require a stronger condition called Harris recurrence, which is generally difficult to verify in the trans-dimensional MCMC set-up (Roberts and Rosenthal, 2006; Hastie and Green, 2012).

However in practice we could tackle this issue by drawing the initial state using a continuous distribution centered around the posterior mode (or other approximations to that such as the maximum likelihood estimate). This strategy is employed in our initialization process. To accelerate the convergence of the chain we initialize the knot points at the empirical quantiles of the data so that more knots are initially placed at data-rich regions. For the remaining parameters the initial values are drawn from appropriate truncated normal distributions centered at their respective maximum likelihood estimates computed given the initial knot configuration.

#### A.4 Tackling label switching

A practical consequence of the properties of the model and its prior is that samples generated by the reversible jump MCMC algorithm are subject to the label switching problem, i.e. the state labels can permute during the MCMC iterations without changing the posterior density. As a result, the MCMC output cannot be directly used for inference about the state specific parameters. To tackle this issue we choose to use the pivotal reordering technique suggested in Marin et al. (2005) and Spezia (2009). More details and comparative review of alternative solutions to this problem can be found therein. An outline of the procedure is as follows. We first run the algorithm in an unconstrained way as proposed above and the knot configuration, which is unaffected by label switching, is estimated at the end of the sampling process as  $\hat{K} = \operatorname{argmin}_K \hat{P}(K|y)$  and  $\hat{R}_K = \frac{\sum_{i=1}^T \mathbf{I}(K^{(i)}=\hat{K})R_{K^{(i)}}}{\sum_{i=1}^T \mathbf{I}(K^{(i)}=\hat{K})}$ , where  $\hat{P}(K|y)$  is directly estimated from the reversible jump MCMC output and  $T$  is the size of the MCMC samples (not including burn-in). Conditioned on  $\hat{K}$ , the state labels of each MCMC samples are reordered such that its Euclidean distance to the sample-based maximum a posteriori (MAP) estimate of the parameters with  $K = \hat{K}$ ,  $\left\| \eta_j(\Theta^{(k)}) - \Theta_{\hat{K}}^{MAP} \right\|$ , where  $\eta_j(\cdot)$  is some permutation of the state-specific parameters and  $j = 1, \dots, N!$ , is minimized. The reordered samples can then be used for posterior inference. However, this method may run into problems when the state-specific (spline) coefficients are similar (i.e. the emission densities are highly overlapping), as we did encounter for the third simulation model (the trimod model). To better distinguish between different possibilities of the state



labels, we propose to consider the 'distance' between the emission densities induced by  $\eta_j(\Theta^{(k)})$  and  $\Theta_{\hat{K}}^{MAP}$ , i.e.

$$\left\| \mathbf{f}_{\eta_j}^{(k)} - \mathbf{f}^{MAP} \right\|, \quad (9)$$

where  $\mathbf{f}_{\eta_j}^{(k)} = (f_{\eta_j^1}^{(k)}(y^{(1)}), \dots, f_{\eta_j^1}^{(k)}(y^{(n)}), \dots, f_{\eta_j^N}^{(k)}(y^{(1)}), \dots, f_{\eta_j^N}^{(k)}(y^{(n)}))$ ,  $\mathbf{f}^{MAP} = (f_1^{MAP}(y^{(1)}), \dots, f_1^{MAP}(y^{(n)}), \dots, f_N^{MAP}(y^{(1)}), \dots, f_N^{MAP}(y^{(n)}))$ . The  $f_{\cdot}^{(k)}(\cdot)$  and  $f_{\cdot}^{MAP}(\cdot)$  are given by equation (1), constructed via the k-th sample and the MAP sample, respectively. Thus for the k-th sample we seek a specific permutation  $\eta_{j^*} = (\eta_{j^*}^1, \dots, \eta_{j^*}^N)$  of the state labels such that (9) is minimised. Our experience suggests that in this challenging scenario it often acts more effectively in finding the "correct" state labels than the original pivotal reordering algorithm.

## B Additional results for the simulation study

In this section we give more details and discuss the performance of the proposed algorithm for our simulation models presented in Section 4. The settings for some unspecified constants used in the algorithm are given in Table 1, whose values were tuned via short pilot runs on the simulated data sets. Some diagnostic plots that are related to the mixing and convergence of the sampler are shown in Figures B.1, B.2 and B.3, where the results for each model are obtained for a randomly selected replication of the simulated data set.

For fixed dimensional moves (moves (a)-(e)), the acceptance rates are controlled at the level of 25% – 40%. We analyzed the traces and running averages for selective parameters across MCMC iterations and found satisfactory mixing patterns in most cases. For the dimension changing moves, the averaged acceptance rates for models 1, 2 and 3 are 0.31%, 0.15%, 0.77% ( $n = 1000$ ) and 0.35% ( $n = 5000$ ), respectively. While it is lower than desired in our simulation cases, we did not detect any apparent convergence issues (see Figures B.1, B.2 and B.3). For Model 2 the acceptance rate can be expected to be lower than for the other two scenarios as it has a larger number of states whose emission distributions have quite different characteristics. In general, a new knot is more likely to be accepted if it contributes to some extent to the fit of all the emission densities. On the other hand, the

Table 1: Constants used for the reversible jump MCMC algorithm.

Model	a	b	$\tau_1$	$\tau_2$	$\tau_3$	$\tau_4$	$\tau_5$	$\alpha$
1	$\min(y^{(n)}) - 10$	$\max(y^{(n)}) + 10$	8	0.24	0.7	2	0.24	0.65
2	$\min(y^{(n)}) - 10$	$\max(y^{(n)}) + 10$	9	0.15	0.5	1.8	0.17	0.65
3 (n=1000)	$\min(y^{(n)}) - 5$	$\max(y^{(n)}) + 5$	0.8	0.11	0.5	2	0.65	0.65
3 (n=5000)	$\min(y^{(n)}) - 5$	$\max(y^{(n)}) + 5$	0.6	0.05	0.6	2	0.5	0.65

degree of precision in the posterior distribution of  $K$  is limiting the achievable acceptance rates for the dimension changing moves. For instance, as  $n$  increases, the posterior for  $K$  is expected to be more concentrated, leading to a generally lower acceptance rate. From the algorithmic perspective this rate is mildly affected by the standard deviation  $\tau$  of the truncated normal distribution or the proposal distribution for  $u_i$  used in the birth move. With the functional form of  $\tau$  fixed, we tested the algorithm for a number of choices of  $\alpha$ , among which those given in Table 1 performed best. We also investigated the use of other potential proposal distributions in the Beta family, but no clear evidence was found in terms of their superiority over the choice  $U(0, 1)$ . A higher acceptance rate for the dimension changing move may be achieved by modifying the current model or the proposal mechanism. For instance, one might consider using a separate knot configuration for each emission density and propose state-specific jump moves, or generating the random variables  $u_i$  used in equation (5) from a more informative proposal distribution such as a truncated normal distribution centred at its maximum likelihood estimate. However, in either scenario the model complexity or the computational effort may increase significantly, which may prevent a successful application of the algorithm in some settings. Though not presented here, we also investigated the estimation performance of the algorithm with other simulation settings. Our preliminary findings indicate that the performance generally improves as serial correlation and/or sample size increases, while it declines as the number of states and/or the overlap of the emission distributions increases.

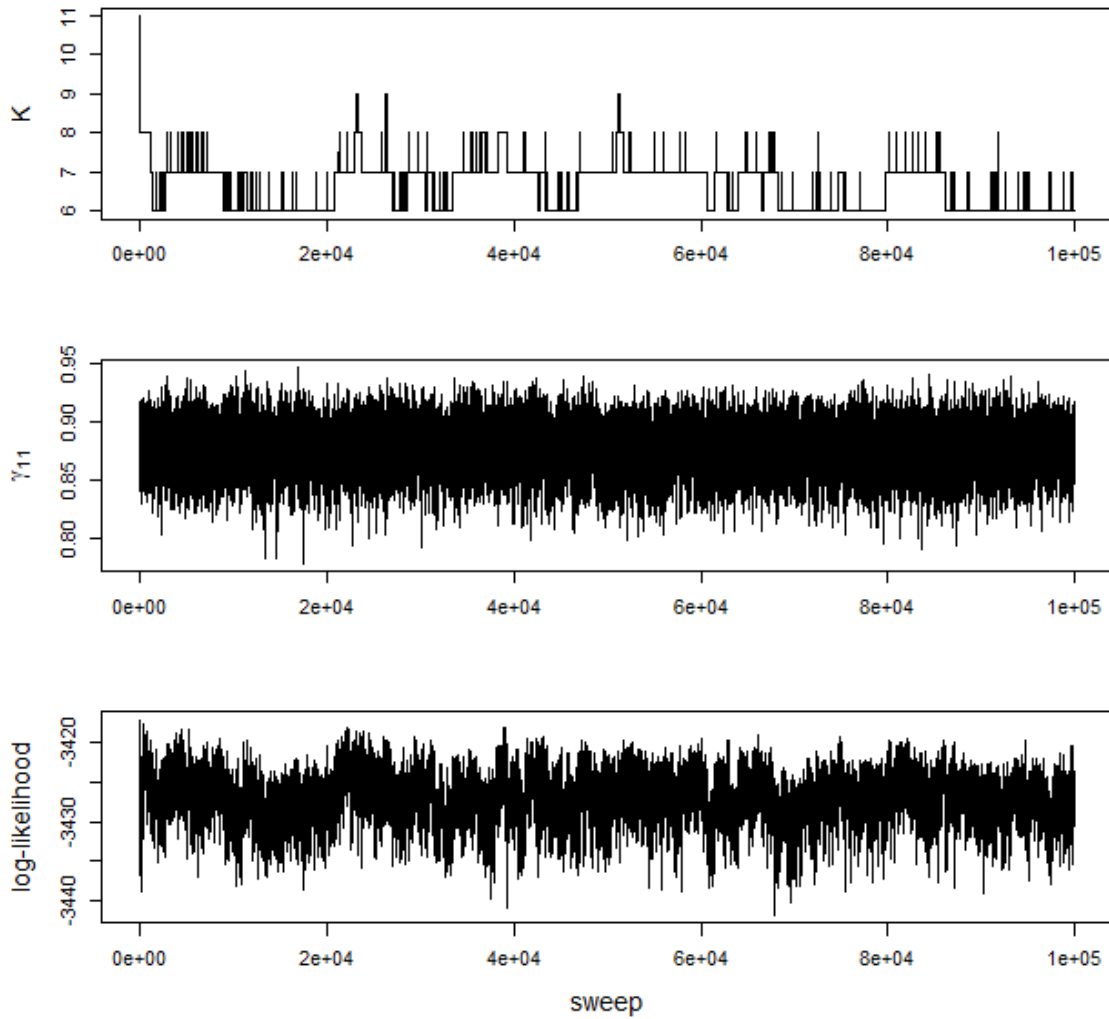


Figure B.1: Results for simulation model 1 conditioned on  $N = 2$ . Top panel: trace of  $K$  for a complete run of 100k MCMC iterations including burn in; middle panel: the corresponding trace for  $r_{11}$  across MCMC iterations; bottom panel: the corresponding log-likelihood of the model generated by the algorithm.

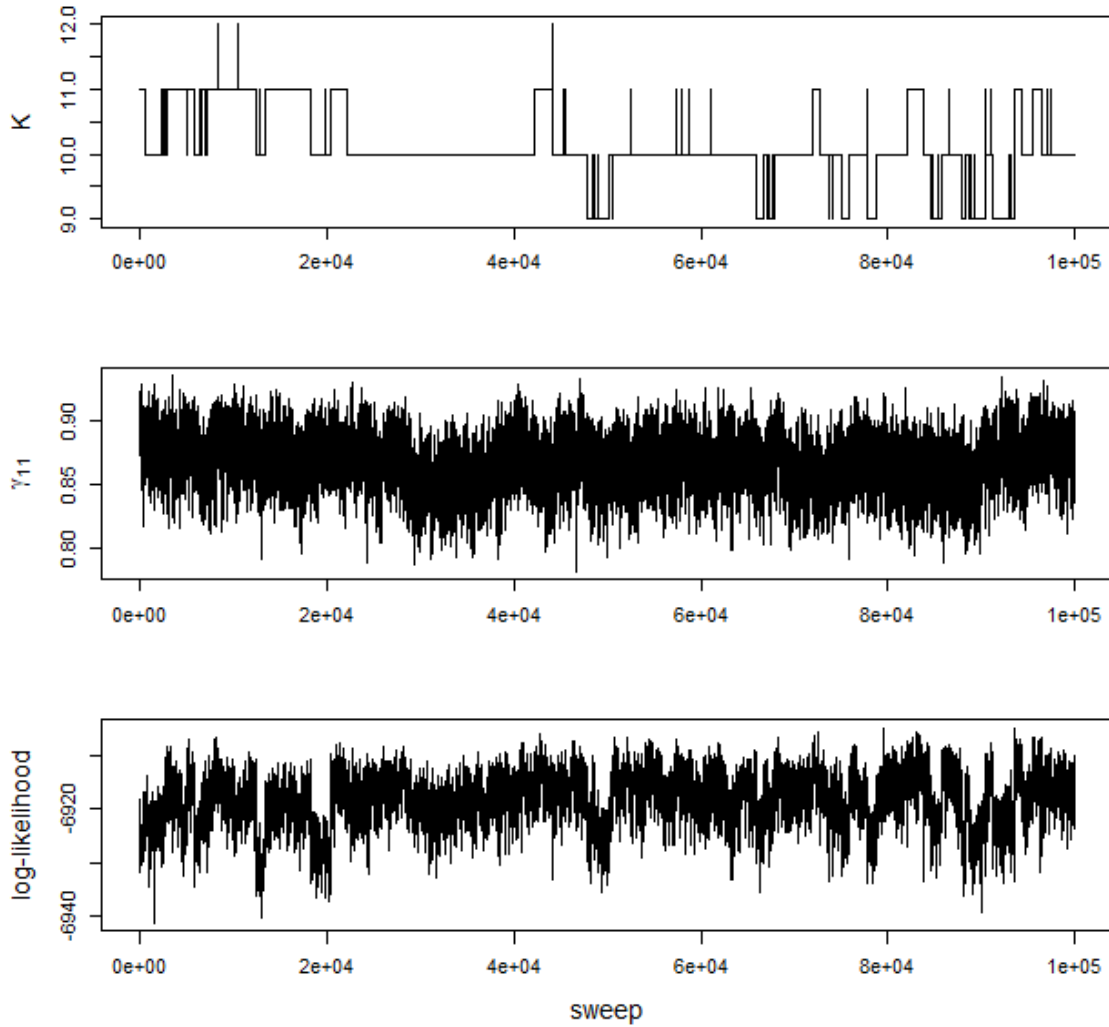


Figure B.2: Results for simulation model 2 conditioned on  $N = 3$ . Top panel: trace of  $K$  for a complete run of 100k MCMC iterations including burn in; middle panel: the corresponding trace for  $r_{11}$  across MCMC iterations; bottom panel: the corresponding log-likelihood of the model generated by the algorithm.

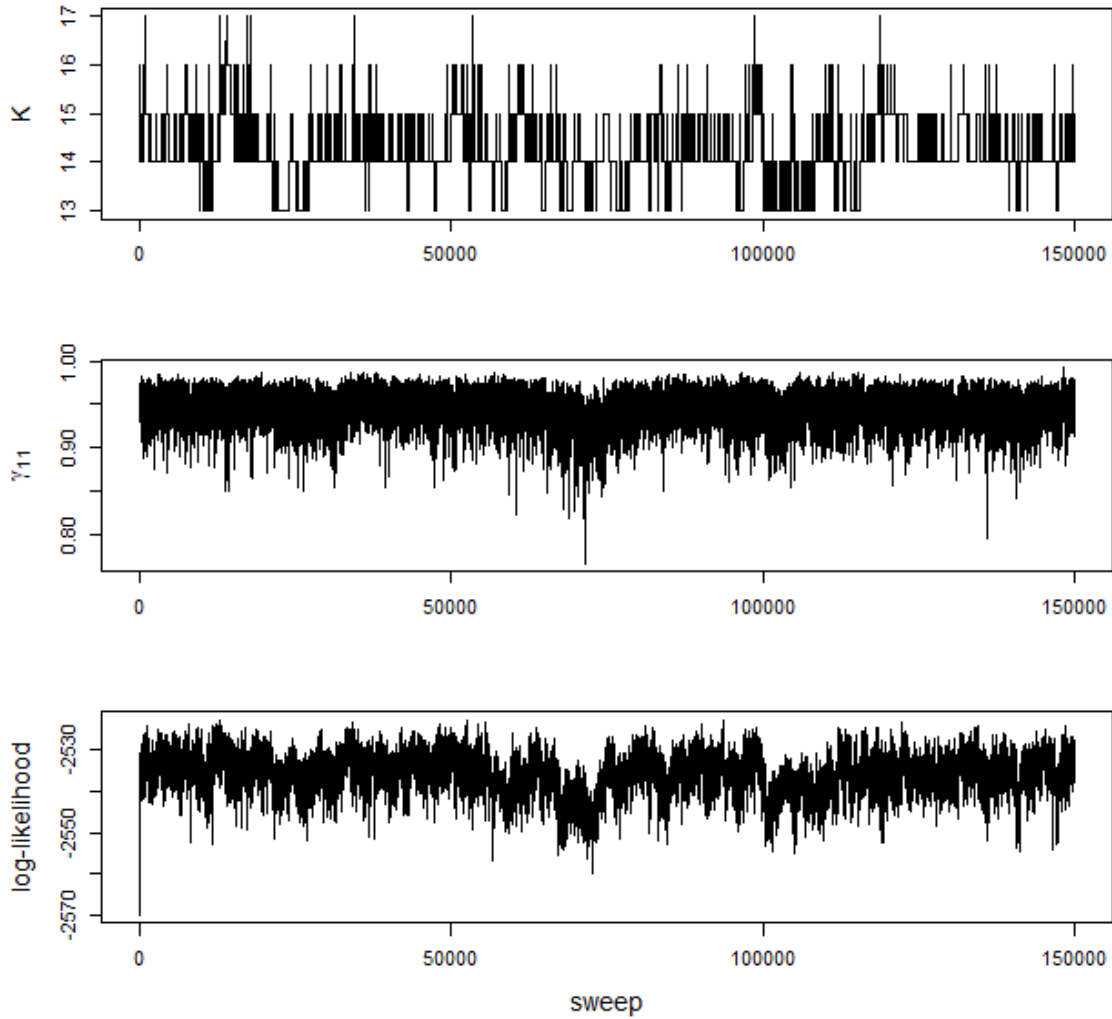


Figure B.3: Results for simulation model 3 ( $n = 1000$ ) conditioned on  $N = 2$ . Top panel: trace of  $K$  for a complete run of 100k MCMC iterations including burn in; middle panel: the corresponding trace for  $r_{11}$  across MCMC iterations; bottom panel: the corresponding log-likelihood of the model generated by the algorithm.

## C Further details of the empirical application of Section 6.1

In this section we provide additional details for the 3 and 7-state HMMs estimated by our proposed method. For the 3-state model, our posterior summaries for the entries of the transition probability matrix are

$$\hat{\Gamma} = \begin{pmatrix} 0.943_{(0.006)} & 0.057_{(0.006)} & 0.001_{(0.001)} \\ 0.029_{(0.003)} & 0.961_{(0.004)} & 0.01_{(0.002)} \\ 0.005_{(0.004)} & 0.048_{(0.01)} & 0.947_{(0.01)} \end{pmatrix},$$

where the point estimates are the posterior means and the associated standard deviations are shown in brackets. In particular, the diagonal entries of  $\hat{\Gamma}$  are all close to 1 highlighting the serial dependence. For the 7-state model, our posterior estimates are based on 50k draws after a burn-in of 50k iterations. Figure C.1 displays the estimated emission densities (left panel) and the Viterbi-decoded times series (right panel) obtained based on posterior means of the model's parameter vector with  $K$  fixed to its posterior mode. We can see that the estimated hidden states roughly correspond to 7 different levels of activity which resolves the multimodality seen in the 3-state model (state 1) into a mixture of unimodal emission densities. Posterior means for the transition probabilities are

$$\hat{\Gamma}_7 = \begin{pmatrix} 0.863 & 0.118 & 0.008 & 0.003 & 0.003 & 0.002 & 0.002 \\ 0.068 & 0.777 & 0.135 & 0.008 & 0.004 & 0.008 & 0.001 \\ 0.017 & 0.117 & 0.69 & 0.137 & 0.02 & 0.017 & 0.002 \\ 0.001 & 0.002 & 0.059 & 0.791 & 0.134 & 0.012 & 0.001 \\ 0.001 & 0.004 & 0.012 & 0.102 & 0.83 & 0.05 & 0.001 \\ 0.004 & 0.019 & 0.047 & 0.038 & 0.072 & 0.775 & 0.045 \\ 0.002 & 0.003 & 0.003 & 0.002 & 0.003 & 0.052 & 0.935 \end{pmatrix}.$$

All of the estimated states are persistent in the sense that there usually is a large probability of staying in the current state (see diagonal entries of  $\hat{\Gamma}_7$ ). In comparison to the 3-state model, the diagonal entries are naturally lower as the shark's movement is now sub-divided into more states. The fitted model with 7 states indicates, for example, that the lower

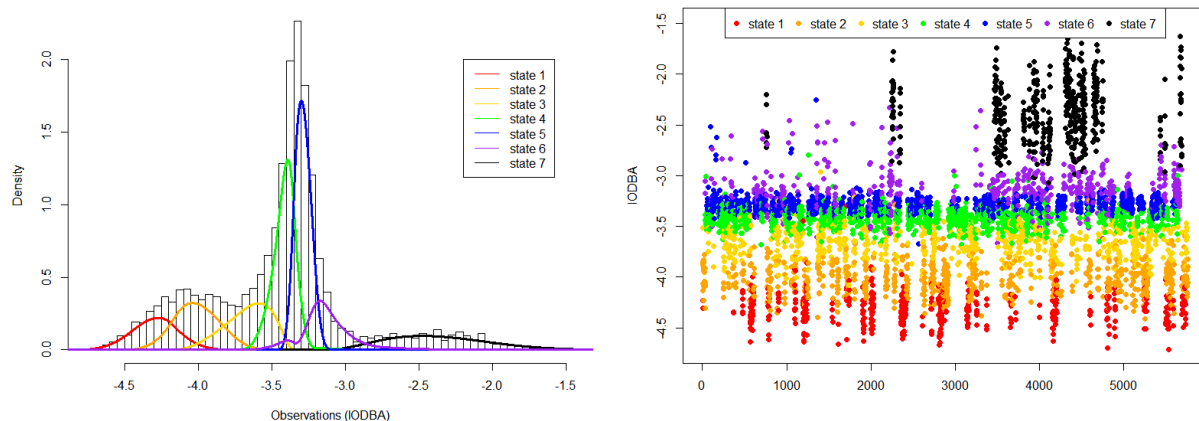


Figure C.1: Left panel: histogram of 15s-averaged IODBA values along with the estimated emission densities (weighted according to their proportion in the stationary distribution of the estimated Markov chain) obtained from our method; right panel: the corresponding Viterbi-decoded time series conditional on the posterior estimate of the parameter of the 7-state model. Here the state labels are sorted according to their mean IODBA levels.

and middle activity mode of the 3-state model can each be associated to several separate states, while the higher activity mode still corresponds to a single state, state 7, whose onset typically occurs following state 6. To assign biologically meaningful interpretations to these states, however, additional specialized information is required and we shall not pursue it further here. Nevertheless, our analysis demonstrates the ability of our method of dealing with model selection in an HMM with a relatively large number of states, while Langrock et al.'s approach may be severely challenged with increasing  $N$ . We also notice that the emission densities of the 7-state model has a fairly regular shape, thus our nonparametric approach could be used in an explorative way to identify a suitable parametric model.

## D Further details of the empirical application of Section 6.2

In this section we present additional implementation details and estimation results for applying the proposed conditional HMM approach on the example subject (subject 9 in Section 6.2).

### D.1 The main HMM

Posterior simulation for the main model can be achieved by using the same MCMC methodology described in Section 3, augmented with an additional Metropolis-Hastings step to update state-specific zero weights  $w_i$ . More specifically, we reparameterize the weights as

$$w_{i,j} = \frac{\tilde{w}_{i,j}}{\tilde{w}_{i,1} + \tilde{w}_{i,2}}, \quad \tilde{w}_{i,j} > 0,$$

where  $w_{i,1}$  corresponds to the probability of observing zero for state  $i$ ,  $i = 1, \dots, N$ ,  $j = 1, 2$ . We choose a vague gamma prior on the  $\tilde{w}_{i,j}$ , i.e.  $f(\tilde{w}_{i,j}) = \text{gamma}(1, 1)$ , which gives a  $\text{Dir}(1, 1)$  distribution on  $(w_{i,1}, w_{i,2})$ . In the MCMC algorithm the  $\tilde{w}_{i,j}$  are updated via a log-normal random walk

$$\log(\tilde{w}'_{i,j}) = \log(\tilde{w}_{i,j}) + \phi_{i,j},$$

where  $\phi_{i,j} \sim \mathcal{N}(0, \tau_6^2)$ . The move is accepted with probability

$$\min\left(1, \frac{f(y^{(n)}|K, R_K, \tilde{A}_K, \tilde{\delta}, \tilde{\Gamma}, \tilde{w}')f(\tilde{w}')}{f(y^{(n)}|K, R_K, \tilde{A}_K, \tilde{\delta}, \tilde{\Gamma}, \tilde{w})f(\tilde{w})} \prod_{i=1}^N \prod_{j=1}^2 \frac{\tilde{w}'_{i,j}}{\tilde{w}_{i,j}}\right),$$

where  $\tilde{w}'$  and  $\tilde{w}$  denote the vectors of proposed  $\tilde{w}'_{i,j}$  and  $\tilde{w}_{i,j}$ , respectively.

In our example, hyperparameters of the prior distributions are specified as  $\epsilon_1 = \epsilon_2 = 1$ ,  $a = 0.1$  and  $b = 362.4$ . Other constants used in the algorithm are taken as  $\tau_1 = 13$ ,  $\tau_2 = 0.3$ ,  $\tau_3 = 0.6$ ,  $\tau_4 = 1.8$ ,  $\tau_5 = 0.22$ ,  $\tau_6 = 0.3$  and  $\alpha = 0.65$  after conducting a few test runs. Our results are based on 50k sweeps of the MCMC algorithm after a burn-in of 50k sweeps. Conditioned on the selected number of states ( $N = 3$ ), the posterior modal number of knots is 6, with  $\hat{P}(K = 6|data) = 0.924$ , and the estimated emission densities (on the positive domain) are displayed in Figure D.1, where the knot sequence and the associated



spline coefficients are estimated by their posterior averages conditional on  $K = 6$ . Our posterior summaries for entries of the transition probability matrix are

$$\hat{\Gamma} = \begin{pmatrix} 0.977_{(0.008)} & 0.02_{(0.008)} & 0.003_{(0.003)} \\ 0.028_{(0.01)} & 0.856_{(0.023)} & 0.116_{(0.021)} \\ 0.004_{(0.003)} & 0.086_{(0.016)} & 0.91_{(0.017)} \end{pmatrix},$$

where the point estimates are the posterior means and the associated standard deviations are shown in brackets.

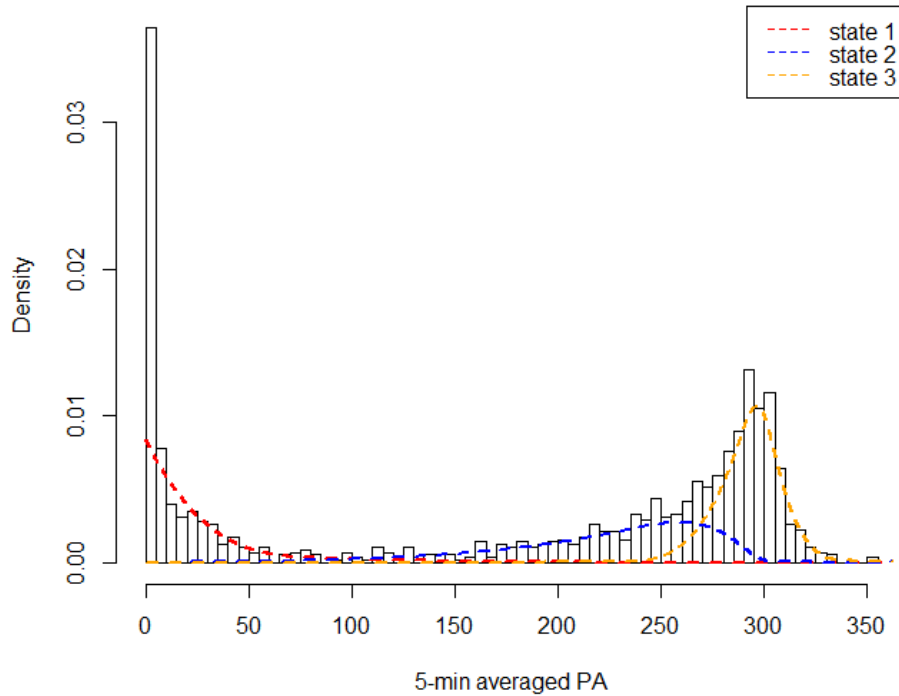


Figure D.1: Histogram of 5-min averaged PA data along with the estimated emission densities (weighted according to their proportion in the stationary distribution of the estimated Markov chain) obtained from our method. The weights at zero for state 1, 2 and 3 are 0.421, 0.003 and 0.002, respectively (not shown in the graph).

## D.2 The sub-HMM

For the sub-HMM, we used the same updating scheme used for the main HMM to update the model parameters including zero weights for each sub-state, and details are omitted here. Hyperparameters of the prior distributions are specified as  $\epsilon_1 = \epsilon_2 = 1$ ,  $a = 1$  and  $b = 323$ . Other constants used in the algorithm are taken as  $\tau_1 = 9$ ,  $\tau_2 = 0.2$ ,  $\tau_3 = 0.7$ ,  $\tau_4 = 1.5$ ,  $\tau_5 = 0.24$ ,  $\tau_6 = 0.25$  and  $\alpha = 0.65$ . Our results are based on 25k samples of  $\Theta_2$  with the first 25k samples discarded as burn-in. The posterior modal number of knots is 3, with posterior probability of 0.97. The estimated emission densities (on the positive domain) for the two sub-states are displayed in Figure D.2, where the knot sequence and the associated spline coefficients are estimated by their posterior averages conditional on  $K = 3$ . Figure D.3 displays the times series of the 1-min position data (measured as the angle formed between the vertical axis and subject's upper body) for each night's sleep bout with colors indicating the Viterbi decoded sub-states from the fitted sub-HMM at each time point. We can see that the occurrences of sub-state 1.2 often coincide with changes in body position.

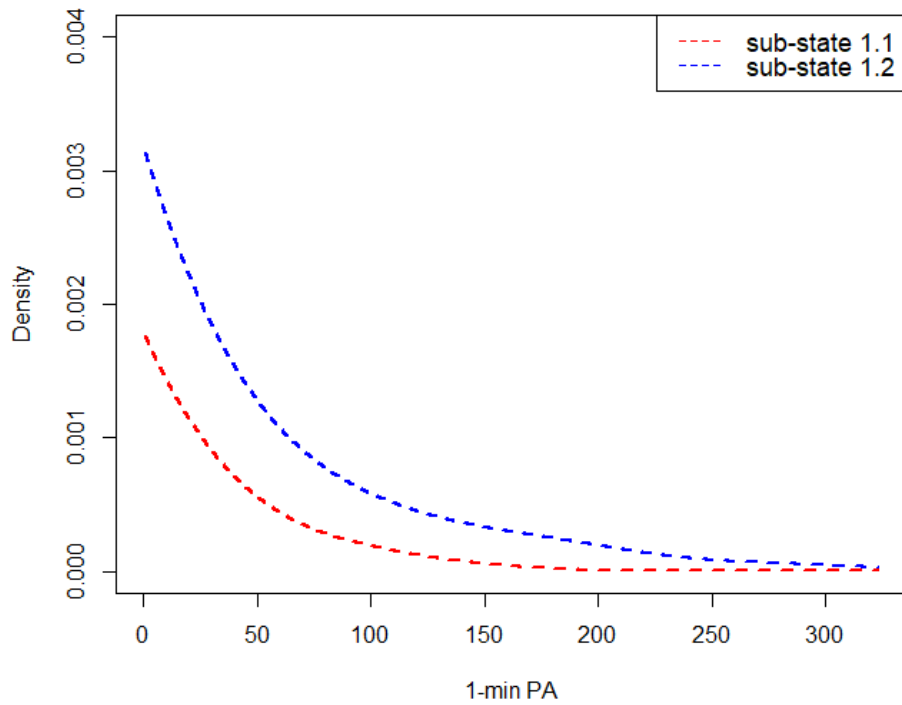


Figure D.2: Estimated emission densities (weighted according to their proportion in the stationary distribution of the estimated Markov chain) obtained from our method. The weights at zero for sub-state 1.1 and 1.2 are 0.898 and 0.246, respectively (not shown in the graph).

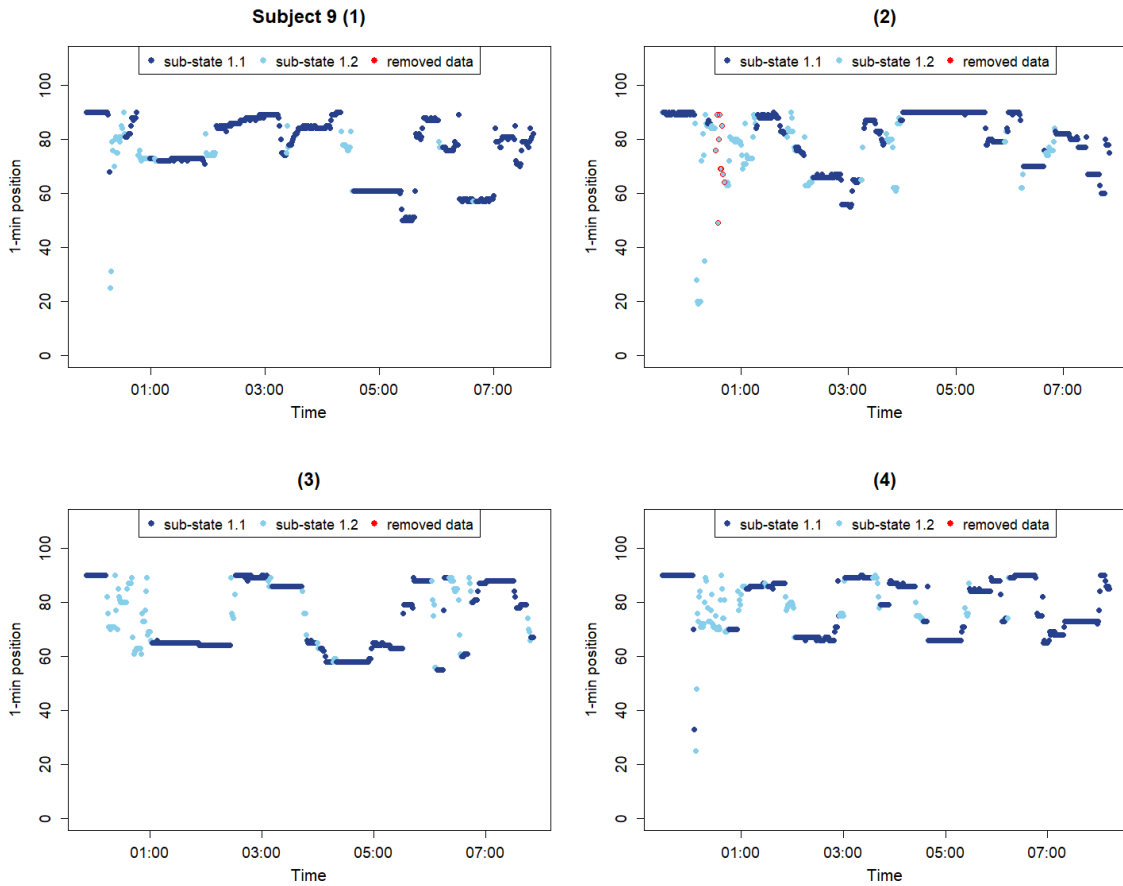


Figure D.3: Panels (1)-(4) display the times series of the 1-min position data for each night's sleep bout with colors indicating the Viterbi decoded sub-states from the fitted sub-HMM at each time point. Removed data (in red) are those that are assigned to a more active state instead of state 1 by the fitted main HMM.

## References

- Green, P. J. (1995). Reversible jump Markov chain Monte Carlo computation and Bayesian model determination. *Biometrika*, 82(4):711–732.
- Hastie, D. I. and Green, P. J. (2012). Model choice using reversible jump Markov chain Monte Carlo. *Statistica Neerlandica*, 66(3):309–338.
- Marin, J.-M., Mengersen, K., and Robert, C. P. (2005). Bayesian modelling and inference on mixtures of distributions. *Handbook of statistics*, 25:459–507.
- Robert, C. and Casella, G. (2013). *Monte Carlo statistical methods*. Springer Science & Business Media.
- Roberts, G. O. and Rosenthal, J. S. (2006). Harris recurrence of metropolis-within-gibbs and trans-dimensional Markov chains. *The Annals of Applied Probability*, pages 2123–2139.
- Spezia, L. (2009). Reversible jump and the label switching problem in hidden Markov models. *Journal of Statistical Planning and Inference*, 139(7):2305–2315.
- Tierney, L. (1994). Markov chains for exploring posterior distributions. *the Annals of Statistics*, pages 1701–1728.